Andradite skarn garnet records of exceptionally low $\delta^{18}O$ values within an Early Cretaceous hydrothermal system, Sierra Nevada, CA

J. Ryan-Davis[1, 2], J.S. Lackey[2], M. Gevedon[3], J.D. Barnes[3],
C-T.A. Lee[4], K. Kitajima[5], J.W. Valley[5]

[1] Geological and Planetary Sciences, California Institute of Technology, Pasadena, California 91125, USA
[2]Geology Department, Pomona College, 185 E. 6th Street, Claremont, California 91711, USA
[3]Department of Geological Sciences, University of Texas, Austin, Texas 78712, USA
[4]Department of Earth Science, MS-126, Rice University, 6100 Main Street, Houston, Texas 77005, USA
[5]WiscSIMS, Department of Geoscience, University of Wisconsin, Madison, Wisconsin 53706, USA

June 18, 2019

Final publication:
Ryan-Davis J, Lackey JS, Gevedon M, Barnes JD, Lee CTA, Kitajima K, Valley JW (2019) Andradite skarn garnet records of exceptionally low $\delta^{18}O$ values within an Early Cretaceous hydrothermal system, Sierra Nevada, CA. Contr. Min. Pet., vol 174. doi.org/10.1007/s00410-019-1602-6

KEYWORDS: skarn, garnet, oxygen isotope, fluid flow, arc magmatism,

ABSTRACT

Skarn garnets in the Mineral King roof pendant of the south-central Sierra Nevada within Sequoia National Park, California, USA reveal variable fluid chemistry with a significant component of meteoric water during metasomatism in the Early Cretaceous Sierra Nevada Batholith. We focus on andradite garnet associated with Pb-Zn mineralization in the White Chief Mine. Laser fluorination oxygen isotope analyses of $\delta^{18}O$ of garnet ($\delta^{18}O(Grt)$) from sites along the skarn show a large range of values (–8.8 to +4.6‰ VSMOW). Ion microprobe (SIMS) analyses elucidate that individual andradite crystals are strongly zoned in $\delta^{18}O(Grt)$ (up to 7‰ of variation). Total rare earth element concentrations ($\sum$REE) across individual garnets show progressive depletion of skarn-forming fluids in these elements during garnet growth.

These findings support a skarn model of earliest red high-$\delta^{18}O$ grandite garnet consistent with a magmatic-dominated equilibrium fluid ($\delta^{18}O(H_2O)$ as high as ≈ +8‰). Later green andradite crystallized in equilibrium with a low-$\delta^{18}O$ fluid indicating a significant influx of meteoric fluid ($\delta^{18}O(H_2O)$ ≈ –6 to –5‰), following a hiatus in garnet growth, associated with late-stage Pb-Zn mineralization. Latest orange overprint rims have higher $\delta^{18}O$ values ($\delta^{18}O(H_2O)$ ≈ 0 to 2‰), and depleted total REEs, suggesting influx of high-$\delta^{18}O$, trace-element depleted fluid derived from regional metamorphism of the carbonate host. Remarkably low $\delta^{18}O(Grt)$ values in the White Chief canyon skarn require a significant proportion of meteoric fluid available during >400°C andradite-forming metasomatism. Fluid flow was channelized at the pluton-wallrock contact, evidenced by the narrow extent of skarn.

ACKNOWLEDGEMENTS

We thank two anonymous reviewers and Executive Editor O. Müntener for their helpful comments that clarified the manuscript. We thank K. Nydick and G. Bradshaw for assistance with permitting for field work in Sequoia National Park, F. Kyte for assistance on the UCLA

electron microprobe, N. Kita, J. Kern and R. Havranek for assistance in the WiscSIMS lab. M. Spicuzza (Wisconsin) and T. Larson (Texas) helped in the LF-IRMS isotope labs. T. Sisson and D. John at the USGS are acknowledged for thoughtful discussions. This work was supported by NSF - OCE-1338842 awarded to Lee, Lackey, Barnes and others as part of the Frontiers in Earth Systems Dynamics program. J. Valley is supported by NSF (EAR-1524336). The WiscSIMS ion microprobe laboratory is supported by the National Science Foundation (EAR-1355590, -1658823) and by the University of Wisconsin–Madison.

INTRODUCTION

Elemental and oxygen isotope zoning within hydrothermal skarn systems is observable at many scales: system-wide across a pluton, outcrop and hand-sample scale, and within individual minerals (e.g., Meinert et al., 2005). Microanalysis by laser ablation or ion microprobe has successfully been used to measure elemental and oxygen isotope compositions within individual garnet crystals from skarns as a precise metric of fluid sources (e.g., Yardley et al. 1991; Jamtveit et al. 1993; Jamtveit and Hervig 1994; Crowe et al. 2001; Clechenko and Valley 2003; Smith et al. 2004; Gaspar et al. 2008; Page et al. 2010; D'Errico et al. 2012). A multitude of properties of the fluids and spatial arrangements in a hydrothermal system (e.g., temperature, fluid-pressure, oxidation state, chemistry, fluid sources, flow rate, diffusion) may be the cause of observable skarn zoning (Bowman 1998b), and therefore a multi-method approach must be used to understand potential causes of zoning in skarns.

This study focuses on a narrow band of andradite-rich skarn at White Chief canyon in the Mineral King Roof Pendant. Pb-Zn-Ag mineralization there drew many miners to the Mineral King mining district in the late 1800's, similar to the rush for gold in the western Sierran foothills but otherwise unique in the Sierra, as most other skarns in the range harbor tungsten mineralization (e.g., Goodyear 1888; Newberry 1982; MacKenzie 1983). The results provide details on the dynamics of garnet chemistry and fluid flow in a shallow, early Cretaceous hydrothermal system in the Sierra Nevada Batholith, a period of magmatic quiescence in the Sierran Arc (Paterson and Ducea 2015), but one that preserves a critical glimpse of hydrothermal

fluid flow in the arc. Comparing oxygen isotope data with from White Chief canyon (this study), with other skarn systems in the same roof pendant, provides a record of changing characteristics of hydrothermal systems at key intervals in the Mineral King roof pendant. These archives of hydrothermal processes give unusual glimpses into upper-crustal fluids in the Cretaceous Sierra Nevada arc. Our investigation of the White Chief canyon skarn has implications for the role of meteoric fluid exchange in the Early-Cretaceous volcanic system.

A comparison of oxygen isotope ratios of garnet, calcite and scheelite ($CaWO_4$) from the White Chief skarn with oxygen isotope ratios measured elsewhere in the pendant tests for contributions of fluids from distal sources (e.g., metarhyolites or metapelites in the pendant). Measured oxygen isotope values whole rock ($\delta^{18}O(WR)$) and zircon ($\delta^{18}O(Zrc)$) from the granodiorite of White Chief Mine provide the best estimates of $\delta^{18}O$ of the magmatic fluid in the skarn-forming system.

We report textural, major, minor, and trace element composition, and oxygen isotope ratios of near-end-member andradite (Adr) garnets from the Pb-Zn White Chief canyon skarn system. By combining petrologic approaches with elemental and isotopic measurements, we provide details of garnet morphology and chemistry that record the evolution of the hydrothermal system including spatial relations of fluid flow over the time period recorded by garnet growth.

GEOLOGIC SETTING

Complex centimeter- to meter-scale mineralogical zoning is apparent in the White Chief Mine skarn within the Mineral King roof pendant in Sequoia National Park (Fig. 1). The Mineral King pendant is among the largest (~10 km^2) roof pendants in the south-central Sierra Nevada batholith (Fig. 1), and is bounded by ca. 98–99 Ma granodiorite and granite plutons (Sisson and

97 Moore 2013). Pendant rocks comprise Triassic-Jurassic metavolcanic and metasedimentary units
98 of the Kings Sequence group (Saleeby and Busby 1993).
99 The pendant also contains early Jurassic (ca. 196 Ma) tuffs and exposes aerially extensive
100 Cretaceous arc volcanic units (132 to 136 Ma) (Klemetti et al. 2014). Small plutons of
101 overlapping age (135 to 136 Ma) are found within and adjacent to the Mineral King pendant and
102 porphyritic textures in dikes and portions of the plutons are common, and provide evidence that
103 the area preserves a shallow "volcano-plutonic suite" transition (Sisson and Moore 2013).
104 Because of this shallow setting, we have assumed that the pressure of skarn formation at White
105 Chief canyon was <1 kbar. Within the metavolcanic units are carbonate-rich units interpreted to
106 represent intervals of volcanic and tectonic quiescence. Pendant protoliths at this location were
107 calcareous quartz sandstone interpreted to have been deposited in a deep marine environment
108 during a break in the volcanic activity that produced the material for the majority of the roof
109 pendant (Busby-Spera and Saleeby 1987; Sisson and Moore 2013). The roof pendant underwent
110 metamorphism and deformation of the volcanic and sedimentary protoliths, assigned to upper
111 greenschist and amphibolite facies (Sisson and Moore 2013), and mineral assemblages in the
112 metamorphic rocks include andalusite and cordierite, suggest low pressure and high temperature
113 associated with pluton emplacement at shallow levels (Sisson and Moore 2013; Klemetti et al.
114 2014). Pressures of 2–3 kilobars are reported by Al-in-hornblende barometry on most of the
115 large, ~98–100 Ma granodiorites that surround the pendant (Ague and Brimhall, 1988). Calcite-
116 and dolomite-rich marbles are exposed to the west and southwest of Empire Mountain, and to the
117 east and northeast of the granodiorite of White Chief Mine (Fig. 1).
118 Hydrothermal exchange between the granodiorite of White Chief Mine and the large
119 marble body that bounds it to the east drove formation of Pb-Zn skarns along a narrow (~1 to 10

120 m wide) zone between the pluton and marble in White Chief canyon (Figs. 1, 2). Field relations
121 indicate that emplacement of the 135±1 Ma (U-Pb zircon, Sisson and Moore 2013) deformed
122 hornblende-biotite granodiorite of White Chief Mine drove skarn formation (Figs. 2 & 3), thus
123 linking its formation to the Early Cretaceous "volcano-plutonic suite" of Sisson and Moore
124 (2013). The White Chief canyon skarns are typically massive garnetites with subordinate green
125 clinopyroxene and in some cases secondary actinolite. Most of the "pockets" of garnetite are
126 composed of red- to beige-colored, granoblastic garnet. Olive-green and orange-rimmed
127 andraditic garnetite, often occurring with up to 80 volume % Pb-Zn sulfide mineralization
128 (galena + sphalerite), occurs as more localized domains within the skarns, with the largest of
129 these being the galena-rich ore zone where White Chief Mine was situated (Fig. 2a). Ore
130 deposition is often associated with late meteoric flooding in skarn systems, which represents the
131 retrograde stage of skarn formation (e.g., Einaudi and Burt 1982; Meinert et al. 2005). This
132 retrograde stage has been the focus of previous work on the White Chief skarn, beginning with
133 ore deposit reconnaissance by J.W. Crabtree in 1873 (Goodyear 1888). MacKenzie (1983)
134 characterized the skarn as a contact-infiltrational exoskarn between the granodiorite and marble.
135 Approximately 5 km to the north-northeast of White Chief canyon (Fig. 1), the 103±4 Ma
136 (Gevedon et al. 2018) skarn system of Empire Mountain, examined by D'Errico et al. (2012),
137 provides an interesting comparison to the White Chief canyon skarn, as both are within the
138 Mineral King roof pendant and indicate meteoric fluid as a major driver of metasomatism and
139 base metal variety in ores. The garnets in each skarn indicate different styles of fluid flow during
140 the skarn-forming intrusions, which are separated in time by nearly 30 million years (Klemetti et
141 al. 2013). Shallow emplacement at ~3.3 km depth of the 106.2 ± 1.1 Ma porphyritic quartz
142 diorite of Empire Mountain (U-Pb zircon, Sisson and Moore 2013)—metasomatically altered the

143 marbles, forming the extensive garnet-rich skarn bodies adjacent to and atop the present
144 exposure of the pluton at Empire mountain (D'Errico et al. 2012).
145 About 4 km north of the granodiorite of White Chief Mine, the small Sequoia Claim
146 skarn (Fig. 1) is thought to be late Cretaceous, in contact with the granodiorite of Castle Creek
147 (U-Pb zircon ages of 97.8 ± 0.7 to 98.4 ± 1.3 Ma (Sisson and Moore 2013)). The time period
148 over which this study examines hydrothermal fluids in the Sierra Nevada arc thus extends
149 through much of the Cretaceous.

150 **METHODS**

151 **Sampling**

152 Samples in this study include skarn, marble, and granodiorite—the main units involved in
153 the hydrothermal system at White Chief canyon and Sequoia Claim skarn (Fig. 2; Table S1
154 Online Resource 1). Thick and thin sections of rock samples were prepared to examine
155 petrographic textures of the rocks and individual garnet crystals. Individual grains, or pieces of
156 large (>1 mm diameter) garnet grains, were liberated from matrix for bulk $\delta^{18}O$ analysis by
157 gently crushing samples by hand in a mortar and pestle. Garnet and other silicate mineral
158 samples were rinsed in dilute hydrochloric acid to remove traces of carbonate and picked by
159 hand to be consistent in color and free of inclusions. A Dremel ® tool was used to rasp powders
160 of calcite from freshly cleaved surfaces of grains in marbles or calcite in skarn. Samples
161 analyzed for bulk rock $\delta^{18}O$ values (Table 1) were prepared from representative 5-10 cm^3
162 domains of the rock trimmed of weathered surfaces and ground in a ring mill with tungsten
163 carbide head for 60–90 s to obtain a uniform, sub-5-µm, powder.

164 **Garnet Morphology and Composition**

Petrographic and scanning electron microscopy guided selection of samples for in situ major, trace, and $\delta_{18}O$ analysis. Garnet grains were first mounted in epoxy and polished to expose grain interiors and then imaged for backscattered electrons (BSE) on the Pomona College Hitachi SU-70 field-emission SEM (15–20 kV accelerating voltage, 38-45 nA beam current, 8-10 mm working distance). Representative garnet crystals were then re-cast in 25.4-mm (dia.) epoxy rounds (Epoxide ® brand) with grains of UWG-2 garnet standard and prepared following the methods described in Valley et al. (1995).

Mounted grains were re-imaged by backscattered electrons and 285 spots on 9 garnet crystals were analyzed for major element chemistry by wavelength dispersive spectrometry using the University of California at Los Angeles JEOL JXA-8200 Superprobe (15 kV,10 nA, 1μm beam diameter). All electron microprobe analytical sessions were calibrated using natural and synthetic mineral standards with counting times of 40 and 10 seconds on peak and background, respectively. Count totals typically varied <1% (2 S.D.) on duplicate samples or standards.

Garnet stoichiometries were normalized to 8 cations and ferrous/ferric iron concentrations were calculated from charge balance. Endmember garnet compositions were calculated as mole percentages, using elemental concentrations of structurally significant elements (Quinn et al. 2016; Table S2 Online Resource 1).

Fluid Inclusion Assemblage Homogenization Temperatures

Fluid inclusions were identified and texturally examined in 100–200 μm thick doubly polished garnet slices. Only homogenization temperatures were obtained via heating microthermometry performed at Pomona College manually with a FLUID, Inc. adapted USGS-type gas flow heating/cooling stage calibrated with natural and synthetic standards for temperature calibration. Fluid inclusions were interpreted according to Goldstein and Reynolds

(1994) and fluid inclusion assemblages (typically 2 to 5 inclusions showing similar morphology and fluid-vapor assemblages) were identified and observed en masse and thermally homogenized, cycled 2 to 3 times, for microthermometric estimates (Table S3 Online Resource 1). Because inclusions were examined for daughter salts and generally found to be two phase (vapor-liquid), salinities were not measured. We use the homogenization temperatures here for estimating the minimum temperature of garnet growth and thus the minimum temperature of formation; salinities of inclusions were not systematically measured.

Stable Isotope Methods

Laser Fluorination

Thirteen fragments of garnet distinguished by color from eleven hand samples from the White Chief canyon skarn, and other samples including one zircon sample, one grain of scheelite and nine samples of calcite from the White Chief skarn, were analyzed for oxygen isotope ratios by isotope ratio mass spectrometry (IRMS) at the University of Texas and the University of Wisconsin Stable Isotope Laboratories (Table 1). Approximately 2 mg of garnet was measured using the laser fluorination method in which samples were heated by a CO_2 laser in the presence of a BrF_5 atmosphere to liberate oxygen (Sharp 1990; Valley et al. 1995). Liberated oxygen was cryogenically purified, and at University of Wisconsin converted to CO_2, before being analyzed on a dual inlet Finnigan MAT 251 mass spectrometer. At the University of Texas, the gas was analyzed as O_2 using a ThermoElectron MAT 253. Whole rocks including tuffs and plutonic rocks were analyzed as powders (2–2.5 mg) by laser fluorination with an airlock sample chamber system at the University of Wisconsin (Spicuzza et al. 1998). Bulk aliquots of zircon were analyzed at U. Wisconsin—using 2-3 mg of hydrofluoric acid-cleaned grains for each analysis—as homogenized powder, to increase fluorination efficiency (Lackey et. al 2008). In order to

check for precision and accuracy of oxygen isotope analyses, analyses of garnet standard UWG-2 ($\delta^{18}O$ value = +5.8‰, Valley et al. 1995, Page et al. 2010) was analyzed at both labs as well as in-house quartz standard "Lausanne-1" ($\delta^{18}O$ value = +18.1‰) at the University of Texas. All $\delta^{18}O$ values are reported relative to VSMOW, where the $\delta^{18}O$ value of NBS-28 is +9.6‰. Precision on all reported isotopic data measured by laser fluorination is ±0.1‰.

Calcite Analyses

For $\delta^{18}O$ and $\delta^{13}C$ analysis of calcite (Cc) and marble samples (n = 16 and n=7, Table 1), 200– 500 micrograms of powdered sample were placed in 12 ml Exetainer vials and flushed with ultra-high purity helium before reaction with concentrated (D = 1.03 g/cm^3) H_3PO_4 for 2 h at 50 °C. Headspace CO_2 was analyzed using a Thermo Gasbench II coupled to a ThermoElectron MAT 253 following the methods of Spötl and Vennemann (2003). Unknowns were calibrated to Carrara marble, NBS-18, and NBS-19. Measured $\delta^{13}C$ and $\delta^{18}O$ values of the standards are each reproducible within ±0.1‰ (2 S.D.). Carbon and oxygen isotope analysis results are reported relative to VPDB and VSMOW, respectively. All stable isotope analyses of calcite were measured at the University of Texas.

SIMS methods

In-situ oxygen isotope analyses of 85 spots (13 μm diameter) on 6 garnet crystals were performed on a CAMECA IMS 1280 high-resolution, multi-collector ion microprobe at the WiscSIMS Laboratory, University of Wisconsin–Madison on two consecutive days (Tables S2, S3, S4 Online Resource 1). Sample standardization required correction for matrix effects (compositionally dependent instrumental mass fractionation, IMF) because of variable garnet

cation chemistry. Five grandite garnet standards (92LEW2, 92LEW7, 92LEW8, 92LEW10 and Grossular SE) that span from X_{Adr} = 0 to 0.91, and provide a highly systematic, quadratic IMF correction curve (Page et al. 2010), were used in conjunction with UWG-2 to conduct standardization (Table S4 Online Resource 1) (Valley and Kita 2009; Page et al. 2010; D'Errico et al. 2012; Kitajima et al. 2016; Quinn et al. 2016). Because some garnet from the White Chief skarns has appreciable Ca-Ti garnet, the combined mole percent of andradite plus Ca-Ti garnet was used for corrections as recommended by Page et al. (2010) (Table S5 Online Resource 1). Nearest EMPA spot neighbors to SIMS spots from equivalent garnet growth bands (e.g., Figs. 4a, b) were used for IMF correction (Table S6, S5 Online Resource 1).

A $^{133}Cs^{+}$ primary ion beam (20 kV total impact voltage) was focused to a diameter of 13μm on the carbon-coated sample surface. Primary ion currents were ca. 1.9 to 2.2 nA. An electron flood gun and the conductive coating assisted in charge compensation. Secondary $^{16}O^{-}$, $^{16}OH^{-}$, and $^{18}O^{-}$ ions were accelerated away from the sample by −10kV and monitored simultaneously on three Faraday cups. Faraday cups are calibrated in the beginning of the session following routine protocol. The intensity of ^{16}O was ~1.5 to 1.7×10^{9} cps depending on the primary beam intensity and chemical composition of garnet (ca. 10^{9} cps/nA). Mass resolving power (MRP, M/ΔM) was ca. 2200 for ^{16}O and ^{18}O, enough to separate hydride interferences on ^{18}O. Higher MRP (~5000) was used for mass 17 to separate ^{17}O from $^{16}O^{1}H$. There is no evidence of significant hydrogrossular or hydroandradite, as OH content is close to background levels (no more than twice the value measured from the nominally anhydrous UWG-2 standards, aside from outliers of SIMS spot 13WC6C_C2 where the hydride content is 9 times the background UWG-2 value, and spot 13WC8_B_16 where it is 3 times the background value; Table S6, Online Resource 1). The magnetic field was regulated by a Nuclear Magnetic

Resonance (NMR) probe with stability of mass better than 10 ppm for 10 hours. Each analysis took ~3.5 minutes, including 10s pre-sputtering, ~60s of automated centering of secondary ions in the field aperture, and 80 s of counting the three peaks simultaneously. Calibrations of the mass spectrometer were performed every 12 hours. Instrument stability during analytical sessions was documented by repeated analyses of the UWG-2 standard that were used to bracket every 10 to 15 unknown spot analyses (see Table S6 Online Resource 1). The 2 S.D. precision on each analysis is calculated as two standard deviations of the two blocks of UWG-2 standards (n=8) that bracket a series of unknowns. The setting used attained an average spot-to-spot reproducibility of ± ~0.25‰ (2 S.D.) for $\delta_{18}O$ on UWG-2 running standard on the days of analysis.

Major and Trace Element Geochemistry of Garnet Crystals

Laser ablation inductively coupled plasma mass spectrometry (LA-ICP-MS) using a New Wave 213 nm laser and a ThermoFinnigan Element 2 magnetic sector ICP-MS system at Rice University were used to obtain trace element chemistry on 42 spots on the 6 garnet crystals selected for SIMS $\delta_{18}O$ analysis (Table S7 Online Resource 1). Reported major, minor and some trace element concentrations were determined on 50-μm spots in medium mass resolution mode ($m/\Delta m$=3000) to resolve argide and oxide isobaric interferences. Trace element concentrations without significant isobaric interferences were measured in low mass resolution mode ($m/\Delta m$=300) to ensure maximum sensitivity, also ~50 μm spots situated in corresponding zones to medium resolution spots. Ablation scans were inspected for "spikes" of elemental concentrations in order to screen for accidental ablation of mineral inclusions in garnet; such spikes were excluded from integrations. Signal conversion to concentrations used external calibration curves based on analyses of USGS glass standards, BHVO-2 g, BIR1g, and BCR-2 g

using the preferred values from Gao et al. (2002). Resulting elemental concentrations (ppm by weight) were converted elements to oxide and normalized to 100%, following the methods outlined by Lee et al. (2008).

RESULTS

Field Relations

The White Chief skarn zone has discontinuous 1 to 20 m wide pockets or "nodes" of garnetite along the 1.5 to 2 km north-south contact between a steeply dipping marble body and the granodiorite of White Chief Mine (Fig. 2). Because the skarn system is exposed along the drainage of the East Fork Kaweah River, skarn and marble can be observed over 200 hundred meters of vertical elevation difference along the side of the pluton. Color differences in garnet (discussed below) show that the majority of garnet is red-brown in color, but that a subordinate green garnet locally occurs in intimate association with Pb-Zn minerals galena and sphalerite. We discuss later the detailed textural relations between the two kinds of garnet, but in general, the green garnet skarn that forms the nexus of mineralization is <10% of total skarn outcrop area and largely focused at the White Chief Mine (Fig. 2)

The main marble body into which skarn was formed show's weak relict bedding that strikes parallel to the contact and dips steeply to the west and southwest (Fig. 2a), and it exhibits grain-size variation in calcite (1mm to 1cm) with a range of color (Fig. 2b). Fine-grained, blue-grey marble with carbonaceous matter occurs in parts of the body distal from skarns and in contact with calc-silicates; alternatively, bleached white, strongly recrystallized marble with trace (<0.5 modal %) diopside and the absence of carbonaceous matter is found adjacent to skarn zones (Fig. 2b-e). Zones of metasomatic replacement of the marble sometimes show intercalation with strongly recrystallized calcite that sharply transitions to marble (Fig. 2c). Locally, sharp,

small-scale bands of garnet and magnetite are vertically oriented in the marble—in cross-section, the cylindrical pipe appears tabular (Fig. 2d).

Near the contact with the pluton, the transitions from granodiorite to skarn to marble occur over distances of < 1 m. Massive garnetite is most typically red and is interpreted to preserve porosity in the garnetite with euhedral crystals on the order of a centimeter growing into the void spaces (Fig. 2f). Granodiorite exhibits sharp contacts with garnetite (Fig. 2e, 2f), often exposed in glacially polished outcrops. The near vertical orientation of skarn features that parallels the contact of marble with the granodiorite of White Chief Mine suggests the skarn formed along the side of the pluton.

White Chief Skarn Garnet Composition, Growth Textures, and Inclusion Assemblages

The grossular-andradite garnets of the White Chief canyon skarn range from $Adr_{26–96}$, with an average of Adr_{91} of core to rim transects across green low-$\delta^{18}O$ zoned garnets. Two distinctive types of garnet-dominated skarn at White Chief are (1) green garnet skarn associated with Pb-Zn mineralization at the White Chief Mine, and (2) more massive, vuggy red garnetite skarn elsewhere along the pluton-marble contact. The pocket of garnetite that was prospected for the White Chief Mine is the only voluminous section of green garnetite, and veins of such garnets cease to be found outside of the green dashed line showing “domains with green” garnet in Figure 2. The mine-area green garnet has olive to yellow-green andradite cores with red-orange to red grandite rims (Fig. 3). Garnet from the southern end of the skarn is red to reddish-brown grandite (Fig. 3b) ($Adr_{14-45}Grs_{50–74}Sps_{1-3}Alm_{2–9}CaTi_{0-2}$; average Adr_{21}; based upon 3 to 10 electron microprobe spots each on garnet fragments from 4 samples, Table S2 Online Resource 1) and coexists with clinopyroxene and magnetite. Red-brown grandite garnet has an average ferrous/ferric ratio ranging from $1.0 \times 10_{-1}$ to $7.4 \times 10_{-1}$. Clinopyroxene from samples near

White Chief Mine is mainly hedenbergite (Fig. 3a, 3f, 3h) and fills fractures and void spaces between garnets, often as in a patchwork texture with calcite around the rims of garnets. Calcite is texturally late, in interstices between clinopyroxene and garnet (Fig. 3c).

Garnet cores from green garnets in the mine area ore zone (Fig. 2a) are usually high in andradite and oscillatory zoned ($Adr_{78-96}Grs_{1-19}Alm_{0-3}Sps_{1-2}Pyp_{0-1}CaTi_{0-2}$; average Adr_{88}) (Figs. 4, 5, Table S2 Online Resource 1). The oscillatory zoned cores have a high concentration of mineral inclusions of magnetite and lead or zinc sulfide along zones in the outermost core (e.g., Fig. 3c; 13WC8-A, Fig. 4), and occasionally patchy blebs of garnet that crosscut zoning (e.g., Fig. 3f; 13WC1-A, Fig. 5). Often, zones of garnet exhibit patchiness or resorption in the core and at the start of overprint rims, delineated by dashed white lines in Figure 4a and Figure 4b.

Orange overprint rims on several of these mine-area garnets (e.g., 13WC8-A, Figs. 3c, 4) are more andraditic ($Adr_{85-96}Grs_{3-16}Alm_{0-3}Sps_{1-2}Prp_{0-1}CaTi_{0}$; average $X_{Adr} = 0.92$) and massive, with little to no visible oscillatory zoning. These orange rims overprint the latest stages of garnet growth, terminating in cracks or void space filled by calcite, and cross-cutting green garnet oscillatory zoning (Figs. 3c, 5a). They often contain small (<3 μm) scheelite inclusions and are lacking in magnetite and sulfide inclusions. It is notable that, out of all samples we observed in detail, the 13WC8 garnet crystals contain the most abundant dark-colored iron oxide and scheelite mineral inclusions that align parallel to growth zones (Figure 4a).

In samples from directly in and around the central mine adit ore zone, garnet is bright green, often in a matrix of galena and sphalerite (Fig. 3d). They have the lowest-andradite zones in their rims ($Adr_{62-98}Grs_{0-36}Sps_{1-2}Prp_{0-1}CaTi_{0}$; average $X_{Adr} = 0.88$) (Sample 13WC1-A Fig. 5, Table S2 Online Resource 1, sample 13WC1-D). These garnets are strongly zoned and variable in composition, with the highest-andradite zones in their cores ($Adr_{83-98}Grs_{0-15}Sps_{1}Prp_{0-1}CaTi_{0}$;

average X_{Adr} = 0.93). All Si in the skarn minerals is found in garnet or clinopyroxene. No wollastonite or quartz has been identified in the skarn.

Garnets in sample 14WC13 in Figure 3a show the most complete record of skarn formation; early massive red-brown grossular garnetite (mainly exposed in the southern end of the skarn) is crosscut by zoned green andradite garnets with red-orange rims (overlapping in composition with green ore-zone garnets, Fig. 3h), and latest red-orange clusters of 1 to 2 mm garnets, with interstitial calcite. Thus, red grossular garnetite in the southern portion of the skarn system formed sequentially before green garnetite observed by the mine adit, and red-orange andradite rims were the latest garnet to grow in the skarn.

Fluid inclusion assemblage homogenization temperatures

Fluid inclusions in garnet were examined in four samples (13WC24, 14WC12, 14WC13 and 14WC17; Table S3 Online Resource 1) for microthermometric estimation of the minimum temperature of garnet growth. Inclusions showing liquid-vapor phases suitable for homogenization temperature measurements are rare and most inclusions appear to be mineral inclusions (likely magnetite and/or scheelite as observed in other thin sections). Three-phase inclusions were observed—fluid inclusions occasionally show vapor only, or liquid-solid (liquid, daughter salt) inclusions, but variability in the assemblage in a given crystal is likely due to alteration or secondary inclusion populations. Many fluid inclusions are necked or deformed, showing extensive strain-induced elongation deformation with 5:1 to 15:1 length to width ratios. Quasi-cubic fluid inclusions suggest negative crystal shapes and conform to oscillatory growth zones visible in garnets (Fig. 3f, g). These inclusions, usually found in unzoned patches, were deemed most likely to be primary, as opposed to obvious bands of secondary inclusions that

crosscut zoning or are aligned with cracks. For these primary two-phase (liquid-vapor) inclusions, the area of the vapor bubble is ~10% of the inclusion.

A variety of samples (Fig. 3e, f, g), from massive green garnetite with late sulfides, to yellow-green euhedral garnets with red-orange overprint rims, were examined (Table S3 Online Resource 1). In some samples, clusters of small reddish garnet are nearly devoid of fluid inclusions. Most fluid inclusions observed were from green andradite garnets. Groups of 2 to 4 apparently pristine inclusions with similar morphology were targeted for homogenization.

The fluid inclusion homogenization temperature range for primary inclusion assemblages in green andradite garnets is consistent with entrapment from 380° to 400° C (samples 13WC24, 14WC13 and 14WC17). The full range for both red and green garnet for homogenization temperatures is 370° to 415°C, but most commonly, the maximum temperature is ~400° C for primary assemblages, which represent about 10% of observed fluid inclusions. Andradite and hedenbergite may coexist in skarn systems over a temperature stability range of ~400 to 900° C, with lower oxygen fugacity in addition to decreasing activity of SiO_2 at lower temperatures (Taylor and Liou 1987; Einaudi 1982). These inclusion assemblages suggest 400° C as a good approximation of the minimum temperature of skarn formation, consistent with andradite and hedenbergite occasionally intergrown in samples from White Chief canyon.

In samples 13WC24, 14WC12 and 14WC17, secondary inclusions are abundant. A growth parallel but slightly curved, and likely compromised, inclusion homogenized at 350° to 360° C. Inclusion assemblages parallel to ubiquitous crosscutting fractures across massive green garnetite range in homogenization temperature from 265° to 290° C, and as low as 210° to 230° C. Garnet growth during skarn formation reached a minimum temperature of 400° C, and based

on fluid inclusion data from secondary inclusions, garnets interacted with fluids as low as ~200° C during later deformation.

Stable Isotope Geochemistry

Skarns

Garnet from non-mineralized red garnetite pockets along the contact with the White Chief pluton measured as crystal fragments by laser fluorination range in $\delta^{18}O$(Grt) values from ~0 to +4.6‰, and varies from $Adr_{14–45}$, with relatively elevated ferric/ferrous ratio compared to green andradite garnets (Figs. 3h, 6a, Table 1, Table S2 Online Resource 1). Garnet in ore-bearing skarn has the lowest measured $\delta^{18}O$(Grt) values with green varieties clustering at –8.8 to –6.2‰ ($Adr_{62–98}$). Comparing SIMS analyses to EMPA major element compositions (Figs. 4a, 5a), these same green garnets have irregular major-element oscillatory zones and orange slightly more ferric rims (Adr_{90} and greater for both irregular and orange zones) with higher $\delta^{18}O$(Grt) values (oscillatory zone $\delta^{18}O$(Grt) values of –8.8 to –6.0‰, and rim $\delta^{18}O$(Grt) values of –5.5 to –2.2‰) (Figs. 4b, 6a). A $\delta^{18}O$ value of 0.0‰ was measured by laser fluorination of a single, otherwise rare, 2.1 mg fragment of scheelite from sample 13WC-12 (Havranek 2014).

Calcite from marbles and skarns shows a wide range of $\delta^{18}O$(Cc) and $\delta^{13}C$(Cc) values with groupings according to lithology (Fig. 6b, Table 1). Calcite from distal marbles shows some exchange and lowering of $\delta^{18}O$ or $\delta^{13}C$ values from typical marine values. Calcite from coarse-grained, bleached white marbles proximal to skarns and lithologic contacts (<3 m) shows lower $\delta^{18}O$(Cc) (8.4 to 12.2‰) and $\delta^{13}C$(Cc) (–1.5 to –0.4‰) values due to the influx of skarn-forming fluids (Fig. 6b). Calcite from skarns define two patterns: values from calcite found in red, non-mineralized garnetites, mainly in vugs, have a narrow range of $\delta^{18}O$(Cc) values from 7 to 8‰

418 with a wide range of lower $\delta_{13}C(Cc)$ values (–5.4 to –9.6‰); calcite in green garnetite has lower
419 $\delta_{18}O(Cc)$ values, less than 5‰, and a similar range of $\delta_{13}C(Cc)$ values (0.1 to –7.8‰) as calcite
420 from red garnetite (Fig. 6b).
421
422 *Igneous Rocks*
423 Analysis of $\delta_{18}O$ values of zircon ($\delta_{18}O(Zrc)$) and whole rock ($\delta_{18}O(WR)$) samples of
424 granodiorite plutons associated with metamorphism of the Mineral King pendant, and of igneous
425 wallrocks in the pendant (Table 1), provides further information about the extent and nature of
426 hydrothermal fluid flow at White Chief canyon. The $\delta_{18}O(WR)$ value of a single sample of the
427 granodiorite of White Chief Mine is 7.2‰ (Fig. 6a); $\delta_{18}O(Zrc)$ from this sample averages
428 6.9±0.1‰. Measured whole rock and zircon $\delta_{18}O$ values of other igneous rocks in the Mineral
429 King area provide additional baseline values of the magmatic $\delta_{18}O$ value and the relative extent
430 of hydrothermal alteration that affected volcanic and plutonic rocks in the pendant. One sample
431 of the ca. 98 Ma granodiorite of Castle Creek, 11MKP-8, from the northwest edge of the pendant
432 (Fig. 1), has a $\delta_{18}O(WR)$ value of 8.1‰. A sample of the gabbro body that runs axially through
433 the center of the pendant and is of presumed Jurassic age, 11MKP-4, has a $\delta_{18}O(WR)$ value of
434 11.1‰. Values of $\delta_{18}O(WR)$ of the 136.5 ± 2.7 Ma Village Rhyolite tuff and 134.2 ± 0.7 Ma
435 Vandever Mountain tuff (Klemetti et al. 2014) are 4.6‰ (11MK-3) and 9.3‰ (11MK-2),
436 respectively. The lower value is similar to $\delta_{18}O(WR)$ values of tuffs from the northern portion of
437 the pendant (D'Errico et al. 2012), whereas the higher value, from the tuff of Vandever
438 Mountain, is greater than previously reported for any metavolcanic unit in the pendant. Values of
439 $\delta_{18}O(Zrc)$ previously measured in zircon from the Village and Vandever Mountain tuffs are 6.8

and 7.3‰, respectively (Klemetti et al. 2014), and average 7.05‰, statistically identical to zircon in the granodiorite of White Chief Mine.

Intracrystalline Garnet Geochemistry

Nine garnet crystals were examined for in situ major element, trace element, and oxygen isotope compositional variations, and details from samples 13WC1 and 13WC8 are shown in Figures 4 and 5. Data for seven other White Chief skarn garnet crystals measured using the same techniques and showing similar isotopic and chemical compositions are reported in Tables S4, S5 and S7 (Online Resource 1). Oscillatory zones within skarn garnets may act as markers of the evolving hydrothermal system during garnet growth and reflect changes in fluid chemistry (e.g. Park, et al. 2017; Ferry, et al. 2014; Zhai, et al. 2014; D'Errico, et al. 2012; Bocchio, et al. 2010; Page, et al. 2010; Gaspar, et al., 2008; Smith, et al. 2004; Clechenko, et al. 2003; Crowe, et al. 2001; Jamtveit, et al. 1993). Areas with fine-scale laminations and oscillatory zoning indicate fast garnet growth rates, and are found between larger "unconformities" that indicate dissolution or resorption, delineated by dashed white lines in Figures 4b and 5b (Yardley et al. 1991; Jamtveit and Andersen 1992; Jamtveit et al. 1993). The relationship between isotopic and chemical shifts within the crystals, and physical changes in morphology and crystal structure within garnets, such as areas of resorption or rapid garnet growth, gives valuable insight into temporal changes in fluid chemistry and physical conditions of fluid flow.

Garnet A from sample 13WC1 (Fig. 5) is representative of other crystals from this sample. This crystal has the highest variation in andradite composition ($Adr_{62–98}$) in yellow-green garnets. The higher-andradite oscillatory-zoned low-$\delta^{18}O$(Grt) core (–8.5 to –8.0‰) is outlined by a distinctive resorption zone and 250-µm outer core with slightly higher $\delta^{18}O$(Grt) (–7.2 to –8.0‰), and a distinctive ~20 µm wide low-andradite rim ($Adr_{72–90}$; $\delta^{18}O$(Grt) = –8.2‰) followed

463 by noticeable resorption filled in by red-orange garnet growth (Fig 4a). Resorption zones host
464 large and abundant inclusions of the main ore minerals, galena and sphalerite.
465 Garnet crystals from sample 13WC8 (e.g. 13WC8-A, Fig. 4, and 13WC8-B, Table S6,
466 Online Resource 1) display the highest variability in $\delta^{18}O$(Grt) values, from oscillatory-zoned red
467 cores with values as low as –8.8‰ and as high as –6.2‰ in select zones, to un-zoned orange
468 rims higher in andradite with values typically ranging from –5.5‰ to –2.2‰, except for a
469 residual patch of oscillatory zoning with low $\delta^{18}O$(Grt) values (Fig. 4b). The transition from the
470 low-$\delta^{18}O$(Grt) core to the higher $\delta^{18}O$(Grt) orange overprint rim is irregular, crossing original
471 zoning. The major cation chemistry of this garnet is relatively homogeneous ($Adr_{78–96}$; average
472 Adr_{87} in the zoned core with higher values and lower oscillatory zones; Adr_{93} in the overprint
473 rim) (Fig. 4; Table S2 Online Resource 1). The zoned garnet contains small (<5μm) dark-colored
474 iron oxide and scheelite mineral inclusions parallel to growth zones.
475 Individual growth zones observed in BSE images or by EPMA have changing garnet
476 major-element chemistry and often have uniform oxygen isotope ratios. Significant shifts in
477 $\delta^{18}O$(Grt) values (about –9 to –6 ‰, to as high as –2‰, Fig. 4a) occur at abrupt morphological
478 transitions—for example, where wavy zones or dissolution features occur (shown by dotted
479 white lines in Fig. 4b). In general, as $\delta^{18}O$(Grt) value increases within individual garnets, X_{Adr}
480 also increases.
481 In transects from core to rim of garnets from sample 13WC8, zones marked by low $\delta^{18}O$
482 garnet (< −8.0‰) are followed by oscillatory zoned growth with gradually increasing $\delta^{18}O$
483 values, until abrupt, fine-scale dissolution features mark a new zone of low $\delta^{18}O$(Grt) (Fig. 4).
484 Late high-andradite orange rims of garnets tend to vary substantially in their oxygen isotope

485 ratios, increasing to the highest measured values (−2.2‰), and these rims overprint oscillatory
486 zoning in BSE images (sample 13WC8A, Fig. 4b).

487 Trace element concentrations along the same transects in these garnets are variable, but
488 the total REE concentration (ΣREE) correlates to the large changes observed in $\delta^{18}O$(Grt) value
489 or garnet color and morphology from core to rim. ∑REE is higher by about one and a half orders
490 of magnitude from chondrite values in garnet cores, and typically decreases through garnet
491 growth (Figure 4d, 5d, Table S7, Online Resource 1).

492 DISCUSSION

493 **$\delta^{18}O$ Composition of Magmas and Their Fluids**

494 Whole rock and zircon $\delta^{18}O$ laser fluorination values of this study record the isotopic
495 compositions of potential fluids that contributed to the White Chief canyon hydrothermal system
496 (Table 1). Lackey and others (2008) showed that measurements of $\delta^{18}O$ in zircon, an early
497 crystallizing phase that also resists sub-solidus alteration, can be used to determine the $\delta^{18}O$
498 composition of the bulk magma. This calculated value for the magma can itself be used to
499 calculate the $\delta^{18}O$ composition of water that would have been dissolved in the melt and
500 represents an idealized "magmatic fluid" in our models, important in establishing the extent of
501 other fluids circulating in the hydrothermal system exchanging with and altering original
502 magmatic $\delta^{18}O$ values. Assuming a near-solidus temperature of approximately 750°C and using
503 the measured $\delta^{18}O$(Zrc) value from sample 13WC-Grd of 6.9±0.1‰ (Table 1), and its SiO_2
504 content of ~69.0 weight percent (Lackey, unpublished), the $\delta^{18}O$ value of water from the original
505 magma was approximately 8.6‰, calculated following Lackey et al. (2008). The measured
506 $\delta^{18}O$(WR) value of the granodiorite sample, is 1.5‰ lower than calculated, confirming that

lower $\delta^{18}O$ fluids have exchanged with minerals in the granodiorite that are subject to sub-solidus alteration (e.g., feldspars, quartz, micas, hornblende). Similar lowering of whole rock $\delta^{18}O$ composition was confirmed in the younger quartz diorite of Empire Mountain by D'Errico and others (2012).

Previously reported $\delta^{18}O$(Zrc) values of coeval tuffs at Mineral King, 6.8 to 7.3‰ (Klemetti et al. 2014), are within error of the $\delta^{18}O$(Zrc) value of the granodiorite of White Chief Mine suggesting that the ca. 134 to 137 Ma coeval granodiorites and silicic volcanic rocks of the pendant had similar magmatic source values of $\delta^{18}O$. Zircon $\delta^{18}O$ values from these volcanic rocks yield calculated $\delta^{18}O(H_2O)$ values of 8.5 to 9.0‰ for magmatic fluid. In general, the $\delta^{18}O$(WR) values calculated for the pluton and coeval tuffs preclude either rock as a source of anomalously low $\delta^{18}O$ magmatic water, and we adopt 8.5‰ as a lower limit for our value of magmatic $\delta^{18}O(H_2O)$ (Figs. 6a, 7b).

The potential for low-$\delta^{18}O$ magmatic fluids emanating from Late Cretaceous intrusive sources, that could overprint the early Cretaceous signatures at White Chief canyon, is evaluated with our analysis of $\delta^{18}O$(WR) compositions of the large (~45 km N-S) ca. 98 Ma Castle Creek pluton (11MKP-8, Fig. 6a). Its $\delta^{18}O$(WR) value of 8.1‰ is similar to a magmatic $\delta^{18}O$(WR) value previously reported farther west in the pluton (7.9‰, Lackey et al. 2008), and is typical of Late Cretaceous granodiorite plutons in the Sequoia region (Lackey et al. 2008). The relatively "normal" $\delta^{18}O$ value for this large pluton suggests that it was not a source of exotic, low-$\delta^{18}O$ magmatic fluids. Moreover, the single $\delta^{18}O$(Grt) value measured in this study from the small Sequoia Claim skarn, adjacent to the granodiorite of Castle Creek, is relatively high

528 (+5.9‰) compared to all $\delta_{18}O$(Grt) values from White Chief canyon skarn samples, and from
529 Empire Mountain skarn samples (Table 1; D'Errico et al. 2012).
530 As with other typical, small-scale skarns in the Sierra Nevada that do not have low-
531 $\delta_{18}O$(Grt) values (Ryan-Davis et al. 2014), we conclude that Late Cretaceous hydrothermal
532 metamorphism in the Mineral King pendant was limited to fluid mixtures that had low meteoric
533 fluid proportions. Far to the south, in the Mojave section of the arc, exceptionally low $\delta_{18}O$
534 values in skarn garnets have also been reported (Gevedon 2019). There and at the White Chief
535 hydrothermal system, unusual ingress and focusing of meteoric water-dominant hydrothermal
536 fluids occurred during skarn formation.

537 **Calcite-Hosted Records of Fluid Sources**

538 Values of $\delta_{18}O_{VSMOW}$(Cc) and $\delta_{13}C_{PDB}$(Cc) from marble and skarn samples (Table 1)
539 provide a means to appraise the nature and extent of infiltration of low-$\delta_{18}O$ fluid in the White
540 Chief hydrothermal system. Devolatilization in a rock-dominated system without infiltrating
541 fluids could lower $\delta_{18}O$ values of silicate-bearing carbonate by no more than 2 to 4‰ (Valley
542 1986; Bowman 1998b). The protolith marble, nearly pure calcite (with only trace silicates),
543 would not shift much more than a few tenths of permil. Isotopic values of calcite from marbles
544 and calcite from red, non-mineralized, high-$\delta_{18}O$(Grt) garnetite, define an array between a
545 marine isotopic signature and the lower limit of "magmatic calcite" that would be in equilibrium
546 with typical igneous fluid (Fig. 6b).
547 Values of $\delta_{13}C$ in calcite in red garnetite samples approach –10‰ (range of –5.4 to –
548 9.6‰). Calculated $\delta_{13}C$ for "magmatic calcite" ranges from –5 to –8‰. Measured $\delta_{13}C$ in calcite
549 may shift by ~1‰ lower than "magmatic calcite" by exchange with, or oxidation of, up to 5%

550 graphitic matter ($\delta_{13}C$ = –30‰) that makes protolith marbles grey. Values higher than
551 "magmatic calcite" suggest a source of carbon from the marbles, which range from –1.5 to
552 +1.6‰. The variation of $\delta_{18}O$(Cc) values in marble is much greater, ranging from 8.4 to 22.0‰
553 (Table 1; Fig. 6b).

554 Model curves for exchange of water-rich fluids (XCO_2 = 0.1 to 0.3) between original
555 sedimentary values and the lower limit of magmatic calcite values (Fig. 6b, this study, Bowman
556 1998a) at 300 to 550°C, enclose these data from red garnetite and marble proximal to the skarn,
557 suggesting a magmatic fluid-dominated system. In contrast, calcite from the low-$\delta_{18}O$(Grt),
558 green, mineralized, garnetite have $\delta_{18}O$(Cc) values <5‰, falling well below the calculated
559 mixing arrays (Fig. 6b). Significantly lower $\delta_{18}O$ values of calcite from green garnetite samples
560 can only be explained by a large proportion of meteoric fluid present (Table 1; Figs. 6b, 7). Fluid
561 from carbonate would not be responsible for low $\delta_{18}O$ values recorded throughout the skarns at
562 White Chief canyon (e.g., D'Errico et al. 2012).

563 At least two externally derived fluids were present in the hydrothermal system. One is
564 low-$\delta_{18}O$ meteoric water (e.g. negative $\delta_{18}O$ value) that falls outside of the mixing arrays and
565 was most important in the discrete pockets of low-$\delta_{18}O$(Grt) green, mineralized garnetite skarn
566 that are volumetrically and spatially smaller compared to the extent of the red garnetite (Fig. 2).
567 A second fluid was more widespread throughout the skarn, indicating a magmatically dominated
568 fluid from the White Chief pluton based on values of $\delta_{18}O$(Cc) in proximal marbles and the red
569 garnetite skarns. Mixtures of green and red garnet at the scale of hand specimens and single
570 crystals (Figs. 3a, 4a) would suggest that these two fluids had high potential to mix.
571 Nevertheless, $\delta_{18}O$ values of garnet and calcite are largely bimodal (Figs. 6, 7). Thus, it appears

572 that the fluids remained largely discrete, offset in their timing of infiltration in the hydrothermal
573 system (Fig. 8)
574
575 **Chemistry of skarn rocks in relation to chemistry and timing of skarn-forming fluids**
576 Figure 7a plots $\delta^{18}O$ fractionation curves for minerals, including green Adr_{90} garnet
577 (yellow line), that would crystallize in equilibrium with $\delta^{18}O(H_2O)$ of –5‰ over the range of
578 temperatures of interest in the skarn (Table S8 Online Resource 1; Online Resource 2). Figure 7b
579 shows the same curves, and red Adr_{60} garnet (yellow line), for equilibrium fluid of +8.5‰, the
580 calculated lower limit of $\delta^{18}O(H_2O)$ for magmatic fluid in the system (Table S8 Online Resource
581 1; Online Resource 2 for discussion of fractionations). Magmatic fluid alone cannot account for
582 measured $\delta^{18}O$(Grt), and must have mixed with meteoric fluid throughout skarn formation, as the
583 curves for pure magmatic fluid do not overlap with garnet analyses at skarn-forming
584 temperatures (>400°C).
585 Early red grossular garnetite toward the south end of the White Chief canyon are
586 interpreted to have a mostly magmatic fluid signature, as they have the highest measured
587 $\delta^{18}O$(Grt) values (above ~2‰, Figs. 2, 7; Table 1, 2). A component of meteoric water must have
588 been available to lower the overall $\delta^{18}O$ value of the fluid in all samples, as none of the values
589 measured in garnet are above a magmatic-fluid equilibrated $\delta^{18}O$(Grt) value of ~5‰ (Table 1).
590 This is in agreement with measurements of late calcite in these samples (Fig. 6b).
591 Late, green, high-andradite garnetite from the ore zone are interpreted to have formed
592 with a large proportion of meteoric fluid present at temperatures as low as ~400° C (Table S3
593 Online Resource 1), lowering the $\delta^{18}O$(Grt) value to below –2‰ (as low as –9‰) in garnets from
594 the mine adit, or below 1‰ in bulk green garnet (Figs. 2, 4, 5, 7; Table 1). Scheelite inclusions

595 are found within rims of garnets and as small late-stage grains interstitial to calcite (MacKenzie
596 1983; Havranek 2014). Fluid in equilibrium with scheelite has a calculated isotopic range
597 (Wesolowski and Ohmoto, 1986) of –4.4‰ at 700°C to –2.8‰ at 400°C (Fig. 6a), calculated
598 from a single measurement of scheelite $\delta_{18}O$ of 0.0‰ (Table 1). The $\delta_{18}O(H_2O)$ range calculated
599 from the $\delta_{18}O$ value of scheelite at this broad temperature range overlaps with that of the low-
600 $\delta_{18}O$ green andradite garnet, suggesting that they were both in equilibrium with meteoric fluid-
601 dominant fluids. Mineralization in skarns has been shown to form during late-stage influx of
602 meteoric fluid into metasomatic systems (e.g. Meinert et al. 2005; Crowe et al. 2001; Bowman
603 1998a; MacKenzie 1983; Einaudi and Burt 1982).
604 The ∑REE in the types of garnet distinguished above corroborate the sequence of fluids
605 inferred from the $\delta_{18}O$ data. Early, red garnetite at the southern end of the skarn has a high-$\delta_{18}O$,
606 high-∑REE composition suggesting dominance of magmatic fluid. Late, green garnetite from
607 near the mine adit has a low-$\delta_{18}O$ composition and low-∑REE signature suggesting dominance
608 of meteoric fluid in the later stages of the skarn. Orange overprint rims on andradite garnets
609 record the waning, end stages of the skarn system, where $\delta_{18}O$ increases but ∑REE is
610 exceptionally low. Metamorphic fluid from regional carbonates, which are low in ∑REE, may
611 have entered the system as magmatic and meteoric fluid sources were depleted. Figure 8
612 schematically shows the possible fluid sources that contributed to the White Chief system, and
613 our interpreted sequence of garnet growth in the skarn, with corresponding changes in $\delta_{18}O$
614 values and ∑REE concentrations.
615

616 **Oxygen isotope record of changing water sources in hydrothermal systems**

617 Based on the paleolatitude of the southern Sierra reconstructed for the Cretaceous from
618 paleomagnetic measurements (Hillhouse and Gromme 2011), we estimate meteoric water would
619 have a $\delta^{18}O$ value of approximately –8‰ according to hydrologic reconstruction of $\delta^{18}O$
620 compositions in the Cretaceous (White et al. 2001). A value of –8.4‰ is given by White et al.
621 (2001) for Middle Cretaceous (105 to 100 Ma) precipitation in the mountain belt representing
622 present day southern Sierra Nevada.
623 The $\delta^{18}O(H_2O)$ compositions of fluid that formed the low-$\delta^{18}O$ andradite varies by ~7‰
624 (–5.5‰ to +1.4‰, assuming equilibrium at constant T = 500°C) with three distinct isotopic
625 ranges: –5.5 to –3.5‰, –2.8 to –1.5‰, and –0.3 to +1.4‰ (Fig. 6a). Assuming a higher
626 equilibrium temperature of 600°C would require slightly lower fluid $\delta^{18}O$ values (~–5.9 to
627 +1.0‰, Figure 6a, Table S9 Online Resource 1). Repeating the same calculation for the bulk
628 $\delta^{18}O$ values of all garnets, the $\delta^{18}O$ composition of equilibrium fluid varies by >12‰ (–5.1 to
629 +7.7‰) assuming 500°C and equilibrium. Most importantly, all of these fluid compositions are
630 significantly lower than the magmatic fluid value of 8.5‰ calculated for magmatic water in
631 equilibrium with granodiorite, requiring infiltration of meteoric fluid throughout all stages of
632 garnet growth in this skarn system (Fig. 8).
633 These calculations of fluid isotopic composition suggest a strikingly large proportion of
634 meteoric fluid was present in the skarn system (> ~70 percent), followed by a shift in the
635 proportion of magmatic or metamorphic fluid (> 30 percent; schematic plot in Fig. 8). Meteoric
636 water with a $\delta^{18}O$ value of –8‰ mixing with ~15 percent magmatic water ($\delta^{18}O$ = +8.5‰, X_{CO2}
637 = 0) would result in a fluid with a $\delta^{18}O(H_2O)$ value around –5.6‰, the lowest of our calculated
638 fluid compositions. Addition of 15 percent of metamorphic fluid with a $\delta^{18}O(H_2O)$ value of
639 +22‰ (i.e., equilibrated with the most pristine low-grade marble) to pure meteoric water would

only increase the $\delta_{18}O(H_2O)$ composition to –3.5‰, assuming an X_{CO2} of 0 as a theoretical end member case. The variability of a $\delta_{18}O(H_2O)$ values calculated from a single crystal, from –5.6 to +1.3‰, requires significant proportions of multiple sources of fluid. To increase the $\delta_{18}O(H_2O)$ to its maximum calculated value from single crystal transects (+1.3‰ at 500°C) requires a significant influx of magmatic water (~60 percent), or metamorphic fluid (~30 percent), mixed with pure meteoric fluid, depending on the initial meteoric to magmatic water proportions.

Endowment of the White Chief Pb-Zn-Ag Ores

The Pb-Zn with associated Ag ores, which brought mining interest into the Mineral King district (Goodyear 1888), occur exclusively with green, low $\delta_{18}O$ andradite garnets, some of which have late, red-orange rims. Because the green garnets are found cross-cutting early, red, ore-barren grossular garnetite, and not distributed in new zones within marbles, we hypothesize that the red garnetite was a locus of relatively high permeability rocks that served as fluid channels for localized flow of meteoric (low-$\delta_{18}O$) mineralizing fluids (Fig. 8). Thus, the red garnetite was important to important first-stage conditioning of the pluton-wallrock contact and served as a site for late-stage endowment of the skarns with Pb-Zn sulfides. Previous detailed petrographic study of the White Chief ore rocks is in agreement, showing that base and precious metal precipitation was relatively late-stage and fracture controlled (MacKenzie 1983). New work has shown that mineralization often occurs late in skarn systems, varying in age by millions of years in some cases such as the Variscan skarns (Burisch et al. 2019). However, recent attempts to date the absolute timing of the second stage of hydrothermal activity by U-Pb in garnet from White Chief canyon have not yet produced a precise age of the late-stage garnets, as

663 Pb mineralization pervades the green garnets, with common lead hindering construction of
664 robust U-Pb isochrons otherwise shown to be useful in other skarn systems in the Mineral King
665 pendant (Gevedon et al. 2018).

666 Grandite garnet in the Pb-Zn-Ag Darwin skarn, (Argus range, eastern California),
667 similarly shows several stages of formation with differing andradite contents, and mineralization
668 may have occurred several million years later than when the Darwin pluton reached its solidus
669 (Newberry et al. 1991). The stages of garnet growth there are associated with early hornfels
670 metamorphism, followed by W and subsequent Pb-Zn sulfide mineralization, which occurred at
671 low temperatures (<425°C). Similarly, mineral inclusions of scheelite and magnetite in garnets
672 from White Chief canyon, and sulfides filling vugs and surrounding garnets suggest an earlier
673 phase of W mineralization, with late-stage Pb-Zn sulfides. Late meteoric fluid as the main
674 metasomatic agent is commonly invoked for mineralization at Pb-Zn skarn systems—it is the
675 likely source of the latest-stage fluids at the Empire zinc skarns in the Central Mining District,
676 New Mexico based on isotopic measurements (Turner and Bowman 1993). The evidence from
677 the White Chief canyon skarn suggests that meteoric fluids may have played a role during a
678 prolonged period of the later stages of skarn development, similar to these other Pb-Zn skarns.

679 **Incursion of meteoric water alongside a sub-volcanic pluton**

680 At White Chief canyon, the meteoric fluid dominated skarn requires a shallow level of
681 emplacement. Alternatively, pre-existing structural controls such as fractures and possibly
682 regional vertical dipping or axial planar features (e.g. Sisson and Moore 2013) may have allowed
683 for infiltration of meteoric water deep into the skarn system; however, the fine-grained and
684 porphyritic texture of the granodiorite of White Chief Mine, and the coeval volcanic rocks in
685 close proximity (Sisson and Moore 2013), corroborate the shallow nature of the system.

Rhyolites similar in age to the granodiorite of White Chief Mine within the Mineral King roof pendant were erupted during a magmatic lull in the Sierra, during a transition from previously island-arc volcanism to a continental arc (Klemetti et al. 2014). This shallow, extensional arc setting allowed for mixing between meteoric surface water and hydrothermal fluids.

Meteoric fluid could have been convected into the system after heat from the intrusion caused decarbonation and increased pore space, further increasing with garnet crystallization, once magmatic overpressures have subsided (Ramos et al. 2018; Mackenzie 1983). Brittle deformation in the late-stage plumbing system could have allowed meteoric water to dominate during sub solidus cooling (Jamtveit and Hervig 1994; D'Errico et al. 2012). Fluid flow would have been directed out of the pluton and up parallel to the skarn-pluton contact (Yardley and Lloyd 1995; Lackey and Valley, 2004; Bowman et al. 2009). Skarn mineralization extends no more than 10 m from the pluton—if hot magmatic fluids were expelled up and away from the pluton, meteoric fluid must then have been convected locally downward into the system along the sides (Fig. 8). That the lowest $\delta_{18}O$ values are concentrated in mineralized areas with the green garnetite shows that this flow was strongly focused into a narrower "plumbing" system within the existing skarn for the most part and did not convert additional marble to skarn.

CONCLUSIONS

Meteoric water was drawn down by convection into the ~135 Ma White Chief canyon skarn system, resulting in exceptionally low recorded oxygen isotope ratios in skarn garnet (–8.8‰). Pulses of garnet growth and resorption with changing isotopic and trace element chemistry provide a fine-scale record of changing fluid conditions in skarn systems. An overall depletion of ∑REE throughout garnet growth and in zones measured within individual crystals implies late-stage dilution of fluids. Thus, multiple fluids, dominated by meteoric fluid but also

including magmatic and other carbonate-influenced fluid, were involved in skarn formation. Magmatic fluid-releasing events that cause pulses of ^{18}O-enriched fluids to enter the system cause chemical changes in garnet as well as observable resorption textures. In the skarn, shallow levels of magma emplacement accompanied by convection of fluids along the pluton-wallrock contact resulted in drawdown of meteoric water into the hydrothermal system.

Collectively, the Mineral King roof pendant skarns chronicle a 38-million-year transition from sub-volcanic to plutonic hydrothermal systems in an evolving magmatic arc where meteoric water is a significant contribution during an arc-wide magmatic lull, and possibly locally extensional setting. The proportion of meteoric water diminished as magmatic flux increased through the middle Cretaceous and engulfed the pendant. Further studies of mineral zoning in skarn systems have potential for understanding tectonic setting in volcanic arcs as well as the rates of decarbonation in Earth history (Lee et al. 2013; Carter and Dasgupta 2015; Lee and Lackey 2015). Findings from this study point to use of skarn systems as a means of testing for broad changes of access to meteoric vs. magmatic fluids in arc hydrothermal systems and more broadly may illuminate tectonic stress fields in arcs

REFERENCES CITED

Ague JJ, Brimhall GH, (1988) Magmatic arc asymmetry and distribution of anomalous plutonic belts in the batholiths of California: effects of assimilation, crustal thickness, and depth of crystallization. Geological Society of America Bulletin 100:912-927

Baumgartner LP and Valley JW (2001) Stable Isotope Transport and Contact Metamorphic Fluid Flow. Reviews in Mineralogy and Geochemistry 43:415-476

Bau M (1991) Rare earth element mobility during hydrothermal and metamorphic fluid–rock interaction and the significance of the oxidation state of europium. Chemical Geology 93:219–230

Bocchio R, Adamo I, Diella V (2010) The profile of trace elements, including the REE, in gem-quality green andradite from classic localities. The Canadian Mineralogist 48:1205-1216

Boden TA, Marland G, Andres RJ (2017) Global, Regional, and National Fossil-Fuel

738 CO_2 Emissions. Carbon Dioxide Information Analysis Center, Oak Ridge National
739 Laboratory, U.S. Department of Energy, Oak Ridge, Tennessee, U.S.A. doi
740 10.3334/CDIAC/00001_V2017
741 Bottinga Y (1969) Calculated fractionation factors for carbon and hydrogen isotope exchange in
742 the system calcite-carbon dioxide-graphite-methane-hydrogen-water vapor. Geochimica et
743 Cosmochimica Acta 33:49-64
744 Bowen GJ, Wilkinson B (2002) Spatial distribution of $\delta^{18}O$ in meteoric precipitation. Geology
745 30:315-318
746 Bowman JR (1998a) Stable-isotope systematics of skarns. In: Lentz, D.R. (ed.), Mineralized
747 Intrusion-related Skarn Systems. Mineralogical Association of Canada Short Course
748 Handbook 26:99-145
749 Bowman JR (1998b) Basic aspects and applications of phase equilibria in the analysis of
750 metasomatic Ca-Mg-Al-Fe-Si skarns. In: Lentz, D.R. (ed.), Mineralized Intrusion-related
751 Skarn Systems, Mineralogical Association of Canada Short Course Handbook 26:1-49
752 Bowman JR, Valley JW, Kita NT (2009) Constraints on mechanisms of oxygen isotopic
753 exchange and isotopic evolution of $^{18}O/^{16}O$-depleted periclase zone marbles in the Alta
754 aureole, Utah—Insights from ion microprobe analysis of calcite. Contributions to
755 Mineralogy and Petrology 157:77-93
756 Burisch M, Gerdes A, Meinert LD, Albert R, Seifert T, Gutzmer J (2019) The essence of time –
757 fertile skarn formation in the Variscan Orogenic Belt. Earth and Planetary Science Letters
758 519:165-170
759 Busby-Spera CJ (1983) Paleogeographic reconstruction of a submarine volcanic center:
760 geochronology, volcanology and sedimentology of the Mineral King roof pendant, Sierra
761 Nevada, California. PhD Thesis. California Institute of Technology, 317 p.
762 Busby-Spera CJ, Saleeby JB (1987) Geologic guide to the Mineral King area, Sequoia National
763 Park, California. SEPM Pacific Section Field Trip Guidebook 56:1–44
764 Carter LB, Dasgupta R (2015) Hydrous basalt-limestone interaction at crustal conditions:
765 Implications for generation of ultracalcic melts and outflux of CO_2 at volcanic arcs. Earth
766 and Planetary Science Letters 427:202-214
767 Clayton RN, O'Neil JR, Mayeda TK (1972) Oxygen isotope exchange between quartz and water.
768 Journal of Geophysical Research 77: 3057-3067
769 Clechenko CC, Valley JW (2003) Oscillatory zoning in garnet from the Willsboro wollastonite
770 skarn, Adirondack Mts, New York: a record of shallow hydrothermal processes preserved
771 in a granulite facies terrane. Journal of Metamorphic Geology 21:771-784
772 Crowe DE, Riciputi LR, Bezenek S, Ignatiev A (2001) Oxygen isotope and trace element zoning
773 in hydrothermal garnets: windows into large-scale fluid-flow behavior. Geology 29:479-
774 482
775 D'Errico ME, Lackey JS, Surpless BE, Loewy SL, Wooden JL, Barnes JD, Strickland A, Valley
776 JW (2012) A detailed record of shallow hydrothermal fluid flow in the Sierra Nevada
777 magmatic arc from low-$\delta^{18}O$ skarn garnets. Geology 40:763–766
778 Easton AJ, Hamilton D, Kempe DRC, Sheppard SMF, Agrell SO (1977) Low-temperature
779 metasomatic garnets in marine sediments. Philosophical Transactions of the Royal Society
780 of London. Series A, Mathematical and Physical Sciences, 286(1336):253-271

781 Einaudi MT, Burt DM (1982) Introduction: terminology, classification, and composition of skarn
782 deposits. Economic Geology and the Bulletin of the Society of Economic Geologists
783 77:745-754
784 Ferry JM, Kitajima K, Strickland A. Valley JW (2014) Ion microprobe survey of the grain-scale
785 oxygen isotope geochemistry of minerals in metamorphic rocks. Geochimica et
786 Cosmochimica Acta, 144:403-433
787 Friedman I, O'Neil JR (1977) Compilation of stable isotope fractionation factors of geochemical
788 interest. US Geological Survey Professional Paper 440-KK:1-49
789 Gao S, Liu X, Yuan H, Hattendorf B, Guenther D, Chen L, Hu S (2002) Determination of forty
790 two major and trace elements in USGS and NIST SRM glasses by laser ablation-
791 inductively coupled plasma-mass spectrometry. Geostandards Newsletter 26:181-196
792 Gaspar M, Knaack C, Meinert LD, Moretti R (2008) REE in skarn systems: a LA-ICP-MS study
793 of garnets from the Crown Jewel gold deposit. Geochimica et Cosmochimica Acta 72:185-
794 205
795 Gevedon M, Seman S, Barnes JD, Lackey JS, Stockli DF (2018) Unraveling histories of
796 hydrothermal systems via U-Pb laser ablation dating of skarn garnet. Earth and Planetary
797 Science Letters, 498:237-246
798 Gevedon ML (2019) On the timing, fluid sources, and behavior of skarn formation: lessons from
799 oxygen isotopes in skarn garnets of the North American Mesozoic Cordilleran arc. PhD
800 Thesis. University of Texas at Austin, 159 p.
801 Goldstein RH, Reynolds TJ (1994) Systematics of fluid inclusions in diagenetic minerals:
802 Society of Economic Paleontologists and Mineralogists Short Course 3, 199 p.
803 Goodyear WA (1888) Inyo, Kern, Los Angeles, San Bernardino, San Diego, Tulare Counties.
804 California Mining Bureau Report 8:643–652
805 Gustafson WI (1974) The stability of andradite, hedenbergite, and related minerals in the system
806 Ca—Fe—Si—O—H. Journal of Petrology 15:455–496
807 Gutzmer J, Pack A, Lüders V, Wilkinson JJ, Beukes NJ, van Niekerk HS (2001) Formation of
808 jasper and andradite during low-temperature hydrothermal seafloor metamorphism,
809 Ongeluk Formation, South Africa. Contributions to Mineralogy and Petrology 142:27-42
810 Havranek R (2014) Fluid Dynamics and Contact Metamorphism Using Scheelite in California.
811 Pomona College. BA Thesis. Pomona College, 51 p.
812 Hillhouse JW, Gromme S (2011) Updated paleomagnetic pole from Cretaceous plutonic rocks of
813 the Sierra Nevada, California: tectonic displacement of the Sierra Nevada block.
814 Lithosphere 3:275-288
815 Jamtveit B (1991) Oscillatory zonation patterns in hydrothermal grossular-andradite garnet:
816 nonlinear dynamics in regions of immiscibility. American Mineralogist 76:1319-1327
817 Jamtveit B, Andersen TB (1992) Morphological instabilities during rapid growth of metamorphic
818 garnets. Physics and Chemistry of Minerals 19:176-184
819 Jamtveit B, Wogelius RA, Fraser DG (1993) Zonation patterns of skarn garnets: records of
820 hydrothermal system evolution. Geology 21:113-116
821 Jamtveit B, Hervig RL (1994) Constraints on transport and kinetics in hydrothermal systems
822 from zoned garnet crystals. Science 263:505-507

Johnson DM, Hooper PR, Conrey RM (1999) XRF analysis of rocks and minerals for major and trace elements on a single low dilution Li-tetraborate fused bead. Advances in X-ray Analysis 41:843–867

Kitajima K, Strickland A, Spicuzza MJ, Tenner TJ and Valley JW (2016) Improved matrix correction of $\delta_{18}O$ analysis by SIMS for pyralspite and Cr-pyrope garnets. Goldschmidt Conference, 1542, Yokohama, Japan.

Klemetti EW, Lackey JS, Starnes J (2014) Magmatic lulls in the Sierra Nevada captured in zircon from rhyolite of the Mineral King Pendant, California. Geosphere 10:66-79

Klemetti EW, Williamson AL, Greene DC, Lackey JS, (2013) Geothermobarometry of the Castle Creek quartz monzodiorite supports rapid Cretaceous subsidence of the Mineral King metamorphic pendant, Sierra Nevada, California. Abstracts with Programs - Geological Society of America 45:610

Kohn MJ, Valley JW (1998) Effects of cation substitutions in garnet and pyroxene on equilibrium oxygen isotope fractionations. Journal of Metamorphic Geology 16:625–639

Lackey JS, Valley JW, Chen JH, Stockli DF (2008) Evolving magma systems, crustal recycling, and alteration in the central Sierra Nevada batholith: the oxygen isotope record. Journal of Petrology 49:1397–1426

Lackey JS, Cecil MR, Windham CJ, Frazer RE, Bindeman IN, Gehrels G (2012) The Fine Gold Intrusive Suite: The Roles of Basement Terranes and Magma Source Development in the Early Cretaceous Sierra Nevada Batholith. Geosphere 8:292–313

Lee C-TA, Lackey JS (2015) Global continental arc flare-ups and their relation to long-term greenhouse conditions. Elements 11:125-130

Lee C-TA, Oka M, Luffi P, Agranier A (2008) Internal distribution of Li and B in serpentinites from the Feather River Ophiolite, California, based on laser ablation inductively coupled plasma mass spectrometry. Geochemistry, Geophysics, Geosystems - G3 9:Citation Q12011

Lee C-TA, Shen B, Slotnick BS, Liao K, Dickens GR, Yokoyama Y, Lenardic A, Dasgupta R, Jellinek M, Lackey JS (2013) Continental arc-island arc fluctuations, growth of crustal carbonates, and long-term climate change. Geosphere 9:21-36

MacKenzie D (1983) Sulfide mineral deposits of the Mineral King mining district, Tulare County, California. M.Sc. Thesis. California State University–Long Beach, 100 pp.

Mascari S (2007) Metamorphism of marbles in the Sequoia National Park region of the Sierra Nevada, CA. B.A. Thesis. College of Wooster, 52 pp.

Matthews A (1994) Oxygen isotope geothermometers for metamorphic rocks. Journal of Metamorphic Geology 12:211-219

Meinert LD, Dipple GM, Nicolescu S (2005) World skarn deposits. In Hedenquist, J.W., Thompson, J.F.H., Goldfarb, R.J. and Richards, J.P., Eds., Economic Geology 100th Anniversary Volume 1905-2005, Elsevier Science B.V., Amsterdam, Volume 1905-2005:299-336

Newberry RJ (1982) Tungsten-bearing skarns of the Sierra Nevada. I. The Pine Creek Mine, California. Economic Geology 77:823-844

Newberry RJ, Einaudi MT, Eastman HS (1991) Zoning and genesis of the Darwin Pb-Zn-Zg skarn deposit, California: A reinterpretation based on new data. Economic Geology 86:960-982

867 Nicolescu S, Cornell D, Södervall U, Odelius H (1998) Secondary ion mass spectrometry
868 analysis of rare earth elements in grandite garnet and other skarn related silicates.
869 European Journal of Mineralogy 10:251–259
870 Page FZ, Kita NT, Valley JW (2010) Ion microprobe analysis of oxygen isotopes in garnets of
871 complex chemistry. Chemical Geology 270:9-19
872 Park C, Song Y, Kang I-M, Shim J, Chung D, Park C-S (2017) Metasomatic changes during
873 periodic fluid flux recorded in grandite garnet from the Weondong W-skarn deposit, South
874 Korea. Chemical Geology 451:135–153
875 Paterson SR, Ducea MN (2015) Arc magmatic tempos: Gathering the evidence. Elements
876 11(2):91-98.
877 Quinn RJ, Valley JW, Page FZ, Fournelle JH (2016) Accurate Determination of Ferric Iron in
878 Garnets. American Mineralogist, 101:1704-1707
879 Quinn, RJ, Kitajima, K, Nakashima, D, Spicuzza, MJ, Valley, JW (2017). Oxygen isotope
880 thermometry using quartz inclusions in garnets. Journal of Metamorphic Geology, 35:
881 231-252
882 Ramos EJ, Hesse MA, Barnes JD, Jordan JS, Lackey JS (2018) Re-evaluating fluid sources
883 during skarn formation: an assessment of the Empire Mountain skarn, Sierra Nevada,
884 USA. Geochemistry, Geophysics, Geosystems, 19(10):3657-3672
885 Ryan-Davis JR, Head DA, Fulton AA, Lackey JS, Barnes JD, Lee C-TA (2014) Skarn garnet
886 records of fluid control of decarbonation and ore type in the California arc. Goldschmidt
887 Abstracts, 2014 2147
888 Saleeby JB, Busby C (1993) Paleogeographic and tectonic setting of axial and western
889 metamorphic framework rocks of the southern Sierra Nevada, California. In: Dunne GC,
890 McDougall K (eds) Mesozoic paleogeography of the Western United States: II, vol.
891 SEPM, Pacific Section 71, pp 197-225
892 Sharp ZD (1990) A laser-based microanalytical method for the in situ determination of oxygen
893 isotope ratios of silicates and oxides. Geochimica et Cosmochimica Acta 54:1353–1357
894 Sisson TW, Moore JG (2013) Geologic map of southwestern Sequoia National Park, Tulare
895 County, California. In: U. S. Geological Survey Open-File Report 2013–1096, Reston,
896 VA, United States, pp 1:24,000
897 Smith MP, Henderson P, Jeffries TER, Long J, Williams CT (2004) The rare earth elements and
898 uranium in garnets from the Beinn an Dubhaich Aureole, Skye, Scotland, UK: constraints
899 on processes in a dynamic hydrothermal system. Journal of Petrology 45:457-484
900 Spicuzza MJ, Valley JW, McConnell VS (1998) Oxygen isotope analysis of whole rock via laser
901 fluorination: An air-lock approach. Geological Society of America Abstracts with
902 Programs 30:80
903 Spötl C, Vennemann TW (2003) Continuous-flow isotope ratio mass spectrometric analysis of
904 carbonate minerals. Rapid Communications in Mass Spectrometry 17:1004–1006
905 Sun S, McDonough W (1989) Chemical and isotopic systematics of oceanic basalts: implications
906 for mantle composition and processes. Geological Society Special Publications 42:313-
907 345
908 Taylor BE, Liou JG (1978) The low-temperature stability of andradite in C-O-H fluids.
909 American Mineralogist 63:378-393
910 Turner DR, Bowman JR (1993) Origin and evolution of skarn fluids, Empire zinc skarns, Central

Mining District, New Mexico, U.S.A. Applied Geochemistry 8(1):9-36
Valley JW (1986) Stable Isotope Geochemistry of Metamorphic Rocks. In: Stable Isotopes in High Temperature Geological Processes. JW Valley, JR O'Neil, and HP Taylor (eds.), M.S.A. Reviews in Mineralogy 16:445-489
Valley, JW (2003) Oxygen isotopes in zircon. In: Hanchar, JM and Hoskin, PWO (eds) Zircon. Reviews in Mineralogy & Geochemistry 53: 343-385
Valley JW, Bindeman IN, Peck WH (2003) Empirical calibration of oxygen isotope fractionation in zircon. Geochimica et Cosmochimica Acta 67:3257–3266
Valley JW, Kita NT (2009) In situ oxygen isotope geochemistry by ion microprobe. In: Fayek M (ed) Secondary Ion Mass Spectrometry in the Earth Sciences, Short Course, vol 41. Mineralogical Association of Canada, pp 19-63
Valley JW, Kitchen N, Kohn MJ, Niendorf CR, Spicuzza MJ (1995) UWG-2, a garnet standard for oxygen isotope ratios: strategies for high precision and accuracy with laser heating. Geochimica et Cosmochimica Acta 59:5223-5231
White T, Gonzalez L, Ludvigson G, Poulsen C (2001) Middle Cretaceous greenhouse hydrologic cycle of North America. Geology 29:363–366
Woodhead J, Hellstrom J, Hergt J, Greig A, Maas R (2007) Isotopic and elemental imaging of geological materials by laser ablation Inductively Coupled Plasma mass spectrometry. Journal of Geostandards and Geoanalytical Research 31: 331–343
Yardley BWD, Lloyd GE (1995) Why metasomatic fronts are really metasomatic sides. Geology 23:53–56
Yardley BWD, Rochelle CA, Barnicoat AC, Lloyd GE (1991) Oscillatory zoning in metamorphic minerals: an indicator of infiltration metasomatism. Mineralogical Magazine 55:357-365
Zhai D-G, Liu J-J, Zhang H-Y, Wang J-P, Su L, Yang X-A, Wu S-H (2014) Origin of oscillatory zoned garnets from the Xieertala Fe-Zn skarn deposit, northern China: In situ LA-ICP-MS evidence. Lithos 190:279–291

FIGURES

Fig. 1 Location and simplified geologic map of the Mineral King roof pendant, south-central Sierra Nevada, California, modified after Sisson & Moore (2013). Mesozoic metavolcanics and metasedimentary rocks make up the majority of the pendant. White areas are Quaternary alluvium and talus; the quartz diorite of Empire Mountain (106.2 ± 1.1 Ma, Sisson & Moore 2013) spans ~8 km north-south, with skarn, mainly garnetite, along the southwest side and as screens and a pendant that makes up the upper 100 m of Empire Mountain. ~3 km to the south-southwest, White Chief canyon exposes the granodiorite of White Chief Mine (135 ± 1 Ma, Sisson & Moore 2013) in contact with marble and calc-silicate, where metasomatism occurred; at this scale, skarn garnet rocks are not distinguished. Figure 2a, delineated by the box, provides detailed geology of White Chief canyon. Specimens collected elsewhere in the Mineral King pendant in this study are located on the map as white circles outlined in black (e.g., Sequoia Claim skarn, SQMK-1)

Fig. 2 Geologic map of White Chief canyon showing field relationships between granodiorite, skarn, and marble. (a) Detailed geologic map of White Chief canyon showing pockets of garnetite skarn between pendant marble and the east contact of the granodiorite of White Chief Mine. Marble color differences are denoted based on field observation. White areas represent Quaternary alluvium and talus. "Garnet Skarn" is restricted to a narrow (1 to 20 m wide) band of garnetite, in contact with the granodiorite and marble, both white and blue-gray. East of the band of marble, calc-silicate with a protolith of Mesozoic metasedimentary or metavolcanic rock is often also metasomatised. Samples are located on the map, with bulk garnet maximum and minimum $\delta_{18}O$ values in red next to the black sample number. Strike and dip of primary bedding features are labeled on the map. Locations of field photos in panels b through f are denoted with camera icons on the map. (b) Transition zone from dark-gray to bleached white marble (c) Contact between marble and a ductile skarn, with proximal garnetite (Grt) and distal clinopyroxene (Cpx), relative to the pluton, and late calcite (Cc). (d) Early magnetite (Mt) on either side of a vertically-oriented band of red garnet, filling a fracture in the marble. Arrow denotes vertical direction in the field. (e) Exposure of garnetite skarn between granodiorite of White Chief Mine and marble. (f) Garnetite skarn, in contact with the porphyritic granodiorite of White Chief Mine; note void spaces of 2–5 cm with euhedral <~1 cm diameter garnet crystals growing into them presumed to be relict porosity from skarn formation

Fig. 3 Textures and compositions of skarn from White Chief canyon; samples indicated on images. (a) Polished slab, showing that early clinopyroxene (Pyx) growth was followed by massive red garnet (Grt) growth, subsequently crosscut by green to yellow-green andradite garnet (Adr) with red-orange overprint rims, and later calcite (Cc) and dark blue-green hedenbergite filling interstices. (b) Transmitted light image of red-brown grandite garnet (Grt) from the southern end of the skarn. (c & d) Transmitted light images of green andradite in garnet-rich (c) and sulfide-rich (d) skarn; in (c) zoned green garnet cores, with red hematite (Ht) staining on rims, and interstitial calcite (Cc). Dark zones in the green cores are typically clusters of small (<15 μm) magnetite inclusions, and small (<10 μm) scheelite inclusions localized in garnet crystals; in (d) galena (Gal), and lesser sphalerite (not pictured), surrounds andradite from the mine adit area. (e) Transmitted light image; massive green andradite exhibiting numerous crosscutting sulfide veins with hematite staining imparting orange discoloration of some garnet. Late hedenbergite fills interstices of sulfides and some garnets and shows strong association with sulfide mineralization. (f) Enlargement of an area of (e) to show secondary fluid inclusions aligned with through-going fractures andradite (dashed black lines), and overprint rims of unfractured orange garnet that meet at triple-junctions containing hedenbergite. (g) Primary fluid inclusions, in addition to many mineral inclusions, exhibit conformable structure along zones of garnet growth; some fluid inclusions are oblique to growth zones, and likely not primary. (h) Ternary plots of all garnet and clinopyroxene cation compositions from this study. Garnet ranges from nearly pure andradite ($Adr_{73–98}$) in mine adit area samples to grandite (Adr_{14-40}) in red-brown garnetite from the southern skarn. Hedenbergite-rich clinopyroxene dominates as interstitial late growth in mine adit area samples

Fig. 4 Geochemistry and $\delta_{18}O$ values of garnet A from sample 13WC8; (a) Binocular, transmitted light (color) image of garnet zoning, showing the green zoned garnet, which appears

yellow, with small dark magnetite inclusions aligned with growth zones, and some white/reflective calcite, sphalerite and galena in resorbed cores. (b) Backscattered electron (BSE) image of garnet zoning. Bright minerals in the resorbed regions in the backscatter image are galena and sphalerite. White and light blue symbols (to locate the blue, out of line symbols along the plotted transect) with numbers represent SIMS spot locations and measured $\delta_{18}O$ values, plotted in (c). Colored circle pairs represent LA-ICPMS spot pairs along the transect, with ∑REE plotted in (d). Dash-dot white lines indicate resorption features or irregular wavy zoning visible in the backscatter image, and are copied onto transects in the following plots. (c) $\delta_{18}O$ measured by SIMS as black or light blue symbols with gray error bars on the left axis, and corresponding mole percent andradite represented by red circles on the right axis, by distance from core to rim (in microns, μm) shows variability. Red, blue and black arrows represent interpreted fluid behavior, tracking $\delta_{18}O$ values. (d) ∑REE concentration measured by LA-ICPMS, as a sum of REEs (La through Lu) in ppm for each analysis pair, plotted along the same transect

Fig. 5 Geochemistry and $\delta_{18}O$ values of garnet A from sample 13WC1; (a) Binocular, transmitted light (color) image of a polished fragment of garnet (white dotted line indicates epoxy covering the crystal), showing the zoned green andradite core, which appears yellow, with small dark magnetite inclusions aligned with growth zones, and the unzoned red-orange andradite overprint rim with scattered small (<5 μm) scheelite inclusions, not visible. (b) Backscatter electron (BSE) image of garnet zoning, annotated with a red transect line from core to rim (A-A'). Late galena followed by sphalerite is the bright mineral at the rim and in resorbed spaces in the BSE image. Small (<10 μm) inclusions of magnetite and scheelite are sparse in the innermost section (before ~800 μm along the transect) of the garnet. Black and light blue symbols (to locate the blue, out of line symbols along the plotted transect) with numbers represent SIMS spot locations and measured $\delta_{18}O$ values, plotted in (c). Colored circle pairs represent LA-ICPMS spot pairs along the transect, with ∑REE plotted in (d). Dash-dot white lines indicate resorption features or irregular wavy zoning visible in the backscatter image, and are copied onto transect plots. (c) Plot of $\delta_{18}O$ measured by SIMS (black or light blue symbols with gray error bars, barely bigger than the symbol) on the left axis, and corresponding mole percent andradite (red circles) on the right axis, by distance from core to rim (in microns, μm). Red, blue and black arrows represent interpreted fluid behavior, tracking $\delta_{18}O$ values; the red arrow with a dashed outline and question mark is an increase in magmatic fluid interpreted from ∑REE, plotted in (d), with no corresponding $\delta_{18}O$ spot. (d) ∑REE concentration in garnet measured by LA-ICPMS (La through Lu) in ppm for each analysis pair measured for a particular zone, plotted along the same transect line

Fig. 6 Oxygen isotope ratios from White Chief skarn and related rocks. (a) $\delta_{18}O$ values of whole rock powders from plutonic and volcanic rocks, garnet fragments, and scheelite. Black capped lines represent calculated $\delta_{18}O$ values of equilibrium fluid over a range in temperatures from 400°C to 600°C. The $\delta_{18}O$ value of fluid is calculated to a wider range of 700 to 400°C for scheelite, as the temperature of its formation, later than garnet, is uncertain. For sample 13WC8, with the widest range in $\delta_{18}O$(Grt) measured by SIMS, the ranges of values are represented by rectangles—the white and light gray rectangles represent analyses within zoned green andradite cores, the dark gray rectangle represents analyses of the red overprint rim. (b) $\delta_{18}O$ and $\delta_{13}C$

values of calcite from marbles and skarn from the White Chief hydrothermal system. Distal marbles are massive and grey with carbonaceous matter from the White Chief area, and white squares represent samples from other areas of the pendant (Other MK). Calcite from skarn garnetite is distinguished as ore-bearing (with green garnet, thick black empty circles) and ore-absent (with red garnet, black filled circles). Reference values of marine carbonates and "magmatic calcite" calculated from equilibrium fluid fractionation are fitted with box-models for the total system assuming equilibrium carbon isotope exchange of fluid over a range of temperatures. Model curves are calculated according to Bowman (1998a, Equation 9) and assume equilibrium fractionation between calcite end-members in marine limestone ($\delta_{18}O$ = 21 to 25‰; $\delta_{13}C$ = 0 to 3‰) and water-rich fluids [X_{CO2} = 0.1 (300°C); 0.3 (550°C)] from which calcite in equilibrium with magmatic fluid ($\delta_{18}O(Cc)$ = 7.5‰; $\delta_{13}C(Cc)$ = –8.0) would precipitate. End-member values are from Bowman (1998a). Hash marks on model curves are fluid-rock ratios used in the models, but likely far underestimate actual fluid fluxes (Bowman 1998a; Baumgartner and Valley, 2001)

Fig. 7 Oxygen isotope fractionations and measured values for garnet relevant to the White Chief canyon skarn system, where the thick black line represents a given water $\delta^{18}O$ value ($X_{CO2} = 0$), and the curves are calculated equilibrium compositions for quartz (dotted blue line), grossular garnet ($Gros_{100}$, dashed red line) and andradite (Adr_{100}, solid green line). The measured values of $\delta^{18}O$(Grt) in red and green garnets, respectively, are plotted as horizontal bars across both panels. (a) A meteoric water-rich fluid $\delta^{18}O$ of –5‰, where garnets are nearly pure andradite (yellow curve, $X_{Adr} = 0.9$), as seen in green ore-zone garnet. The yellow curve here nearly overlaps the equilibrium andradite curve, in green, and overlaps with measured green garnetite $\delta^{18}O$(Grt) values to temperatures as low as ~400°C, corresponding well to the minimum temperature of 400°C from fluid inclusion assemblages in green garnetite. (b) Magmatic water ($\delta^{18}O = +8.5$ calculated from zircon from the granodiorite of White Chief Mine) results in equilibrium $\delta^{18}O$(Grt) values that are above the highest measured values for the red garnetite. The yellow curve represents the calculated fractionation of Adr_{60} garnet in equilibrium with purely magmatic water ($\delta^{18}O = +8.5$). The yellow curve just intersects the highest red garnetite measured values only at T < 400°C; instead of such a low T of formation of the skarn, it is likely that all garnets formed in fluids that contained some portion of meteoric water, which would lower the curves to meet the measured values at an appropriate skarn-forming temperature range (>400 °C, from fluid inclusion microthermometry)

Fig. 8 Schematic model of skarn formation at White Chief Mine. In the shallow arc setting of ca. 135 Ma, this shallow system drove convection of meteoric fluids into the skarn-forming hydrothermal system at the contact of the pluton with carbonates. Silicic magma of the granodiorite of White Chief Mine intruded carbonate, causing devolatilization of CO_2:H_2O fluid, which was first dominantly magmatic fluid (1). The opening of pore space along the contact formed a conduit for later fluids, *i.e.,* meteoric water (2), and potentially also including metamorphic fluid in equilibrium with local carbonates (3?).

Early red grossular-rich garnet crystallized in the southern present-day exposures of the skarn, with the highest $\delta^{18}O$(Grt) measured, up to > 4‰, and elevated ∑REE. Magmatic fluid ($\delta^{18}O$ of ~+8.5‰) dominated the early red garnet growth, but a significant proportion of meteoric fluid was certainly present (see Figure 7). Diminishing expulsion of magmatic water later allowed low-$\delta^{18}O$ meteoric fluid ($\delta^{18}O$ of –5‰) to flood the system, recorded by low-$\delta^{18}O$, moderate-∑REE green, oscillatory zoned garnet in the ore zone near where abandoned mine adits exist today ($\delta^{18}O$(Grt) < –8‰). Resorption and overprinting of some green zoned garnet cores resulted in red-orange andradite (Adr_{93}) overprinted rims of the garnet during the low-temperature (as low as ~400°C) skarn formation during final stages of cooling of the granodiorite of White Chief Mine, recording pulses of higher-$\delta^{18}O$, low ∑REE fluid (brown and purple bar in $\delta^{18}O$ plot, and pale yellow bar in ∑REE plot), likely a signature of "metamorphic" fluids from regional carbonate rock ($\delta^{18}O$ up to +22‰), recorded by a prominent increase in $\delta^{18}O$(Grt) (> –3‰) and extremely depleted ∑REE within the red-orange andradite garnet rims

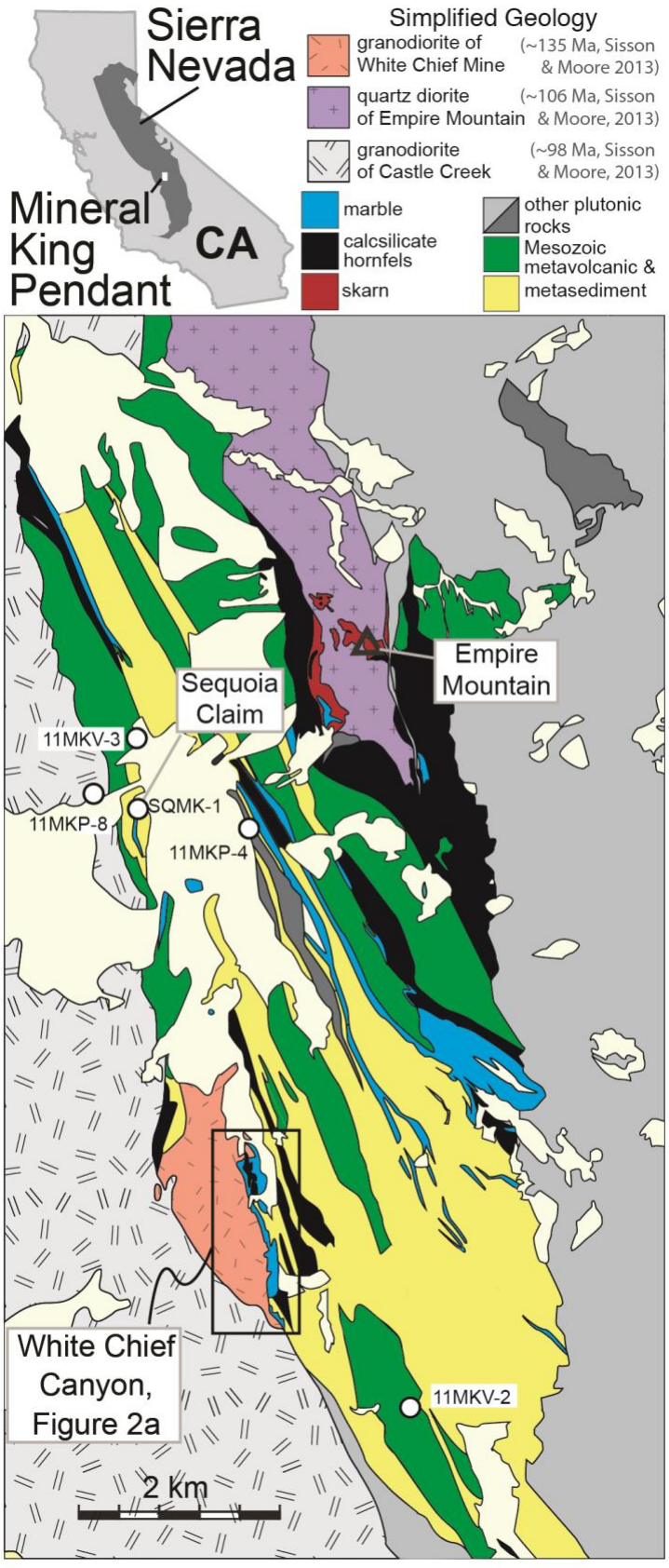
Sierra Nevada
Mineral King Pendant
CA
Simplified Geology
granodiorite of White Chief Mine
(~135 Ma, Sisson & Moore 2013)
quartz diorite of Empire Mountain
(~106 Ma, Sisson & Moore, 2013)
granodiorite of Castle Creek
(~98 Ma, Sisson & Moore, 2013)
marble
calcsilicate hornfels
skarn
other plutonic rocks
Mesozoic metavolcanic & metasediment
Empire Mountain
Sequoia Claim
11MKV-3
11MKP-8
SQMK-1
11MKP-4
White Chief Canyon, Figure 2a
11MKV-2
2 km

Fig. 1 Location and simplified geologic map of the Mineral King roof pendant, south-central Sierra Nevada, California, modified after Sisson & Moore (2013). Mesozoic metavolcanics and metasedimentary rocks make up the majority of the pendant. White areas are Quaternary alluvium and talus; the quartz diorite of Empire Mountain (106.2 ± 1.1 Ma, Sisson & Moore 2013) spans ~8 km north-south, with skarn, mainly garnetite, along the southwest side and as screens and a pendant that makes up the upper 100 m of Empire Mountain. ~3 km to the south-southwest, White Chief Canyon exposes the granodiorite of White Chief Mine (135 ± 1 Ma, Sisson & Moore 2013) in contact with marble and calc-silicate, where metasomatism occurred; at this scale, skarn garnet rocks are not distinguished. Figure 2a, delineated by the box, provides detailed geology of White Chief Canyon. Specimens collected elsewhere in the Mineral King pendant in this study are located on the map as white circles outlined in black (e.g., Sequoia Claim skarn, SQMK-1)

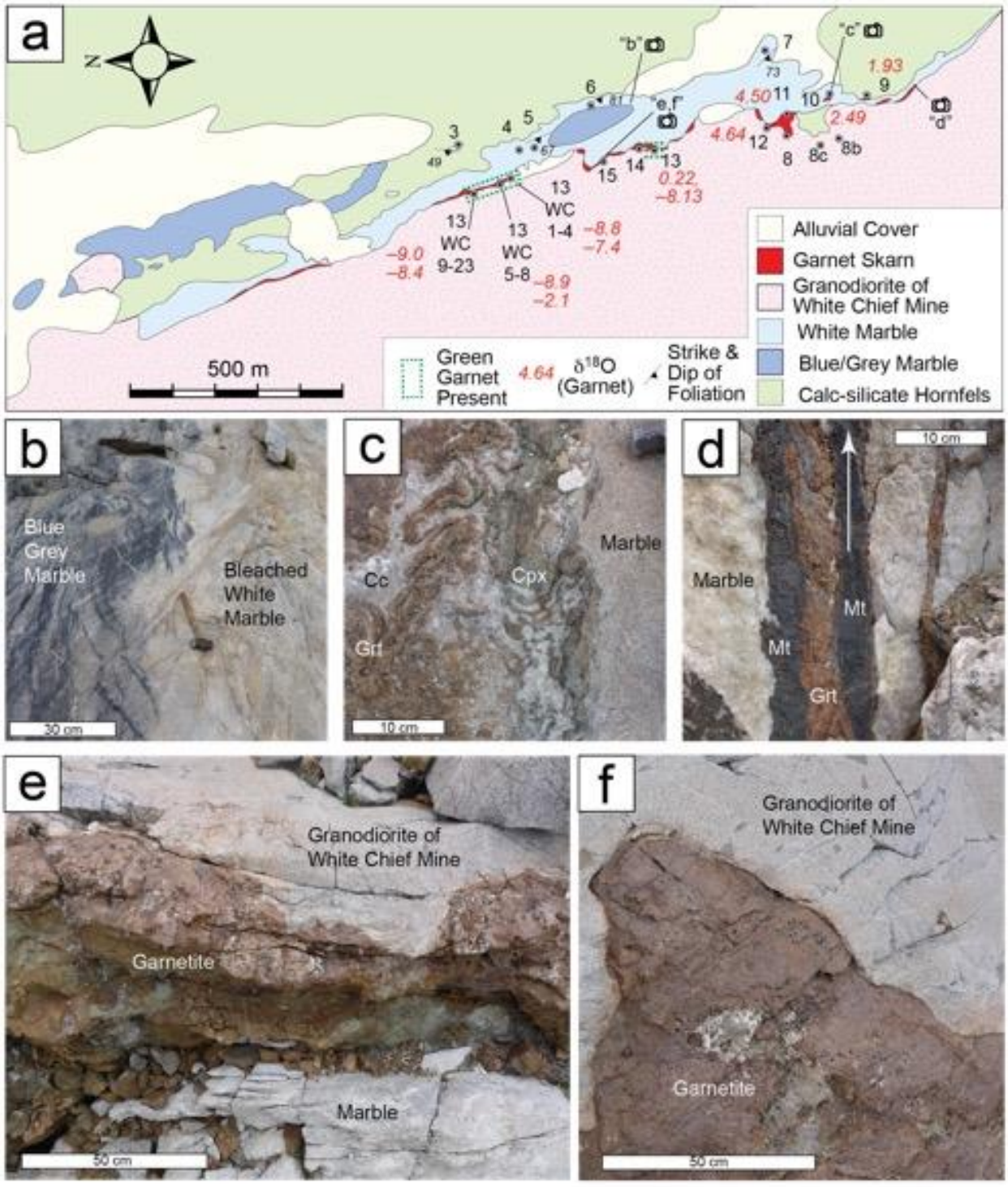

Fig. 2 Geologic map of White Chief Canyon showing field relationships between granodiorite, skarn, and marble. (a) Detailed geologic mapping of White Chief Canyon showing pockets of garnetite skarn between pendant marble and the east contact of the granodiorite of White Chief Mine. Marble color differences are denoted based on field observation. White areas represent Quaternary alluvium and talus. "Garnet Skarn" is restricted to a narrow (1 to 20 m wide) band of garnetite, in contact between the granodiorite and marble, both white and blue-gray. Calc-silicate

east of the band of marble with a protolith of Mesozoic metasedimentary or metavolcanic rock is often also metasomatised. Samples are located on the map, with bulk garnet maximum and minimum $\delta_{18}O$ values in red next to the black sample number. Strike and dip of primary bedding features are labeled on the map. Locations of field photos in b-f panels are denoted with camera icons on the map. (b) Transition zone from dark-gray to bleached white marble (c) Contact between marble and a ductile skarn, with proximal garnetite (Grt) and distal clinopyroxene (Cpx), relative to the pluton, and late calcite (Cc). (d) Early magnetite (Mt) on either side of a vertically-oriented band of red garnet, filling a fracture in the marble. Arrow denotes vertical direction in the field. (e) Exposure of garnetite skarn between granodiorite of White Chief Mine and marble. (f) Garnetite skarn, in contact with the porphyritic granodiorite of White Chief Mine; note void spaces of 2–5 cm with euhedral ~cm scale garnet crystals growing into them presumed to be relict porosity from skarn formation

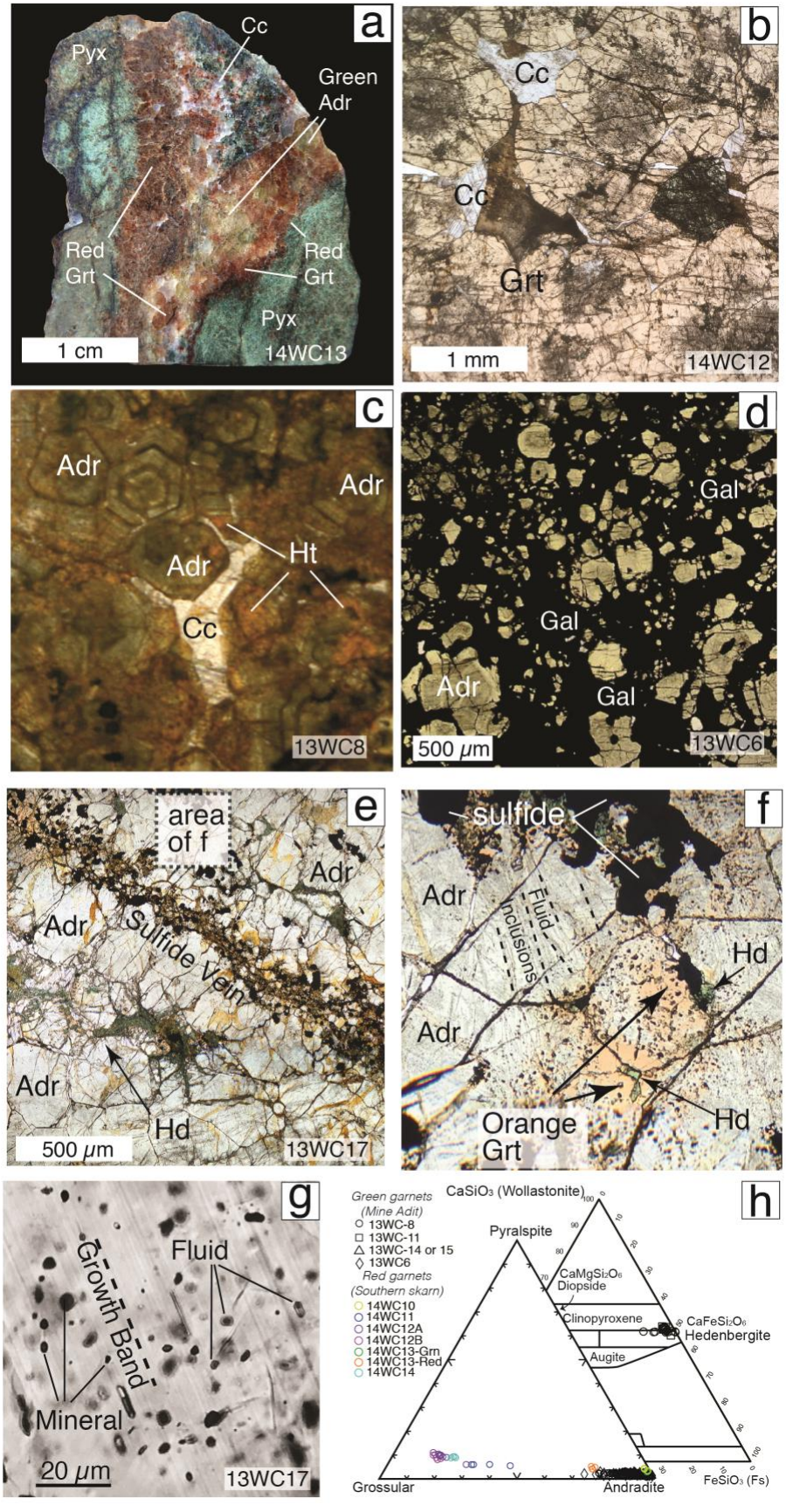
a
Cc
Pyx
Green
Adr
Red
Grt
Red
Grt
Pyx
1 cm
14WC13
b
Cc
Cc
Grt
1 mm
14WC12
c
Adr
Adr
Adr
Ht
Cc
13WC8
d
Gal
Gal
Adr
Gal
500 μm
13WC6
e
area
of f
Adr
Adr
Sulfide Vein
Adr
Hd
500 μm
13WC17
f
sulfide
Adr
Fluid
Inclusions
Hd
Adr
Orange
Grt
Hd
g
Growth Band
Fluid
Mineral
20 μm
13WC17
h
Green garnets
(Mine Adit)
13WC-8
13WC-11
13WC-14 or 15
13WC6
Red garnets
(Southern skarn)
14WC10
14WC11
14WC12A
14WC12B
14WC13-Grn
14WC13-Red
14WC14
CaSiO3 (Wollastonite)
Pyralspite
CaMgSi2O6
Diopside
Clinopyroxene
CaFeSi2O6
Hedenbergite
Augite
Grossular
Andradite
FeSiO3 (Fs)

Fig. 3 Textures and compositions of skarn from White Chief canyon; samples indicated on images. (a) Polished slab, showing that early pyroxene (Pyx) growth was followed by massive red garnet (Grt) growth, subsequently crosscut by green to yellow-green andradite (Adr) with red-orange overprint rims, and later calcite (Cc) and dark blue-green hedenbergite filling interstices. (b) Transmitted light image of red-brown grandite garnet (Grt) from the southern end of the skarn. (c & d) Transmitted light images of green andradite in garnet-rich (c) and sulfide-rich (d) skarn; in (c) zoned green garnet cores, with red hematite (Ht) staining on rims, and interstitial calcite (Cc). Dark zones in the green cores are typically clusters of small (<15 μm) magnetite inclusions, and small (<10 μm) scheelite inclusions localized in garnet crystals; in (d) galena (Gal), and lesser sphalerite (not indicated), surrounds andradite from the mine adit area. (e) Transmitted light image; massive green andradite exhibiting numerous crosscutting sulfide veins with hematite staining imparting orange discoloration of some garnet. Late hedenbergite fills interstices of sulfides and some garnets and shows strong association with sulfide mineralization; (f) enlarges an area of (e) to show secondary fluid inclusions aligned with through-going fractures andradite (dashed black lines), and overprint rims of unfractured orange garnet that meet at triple-junctions containing hedenbergite. (g) Primary fluid inclusions, in addition to many mineral inclusions, exhibit conformable structure along zones of garnet growth; some fluid inclusions are oblique to growth zones, and likely not primary. (h) Ternary plots of all garnet and clinopyroxene cation compositions from this study. Garnet ranges from nearly pure andradite ($Adr_{73–98}$) in mine adit area samples to grandite (Adr_{14-40}) in red-brown garnetite from the southern skarn. Hedenbergite-rich clinopyroxene dominates as interstitial late growth in mine adit area samples

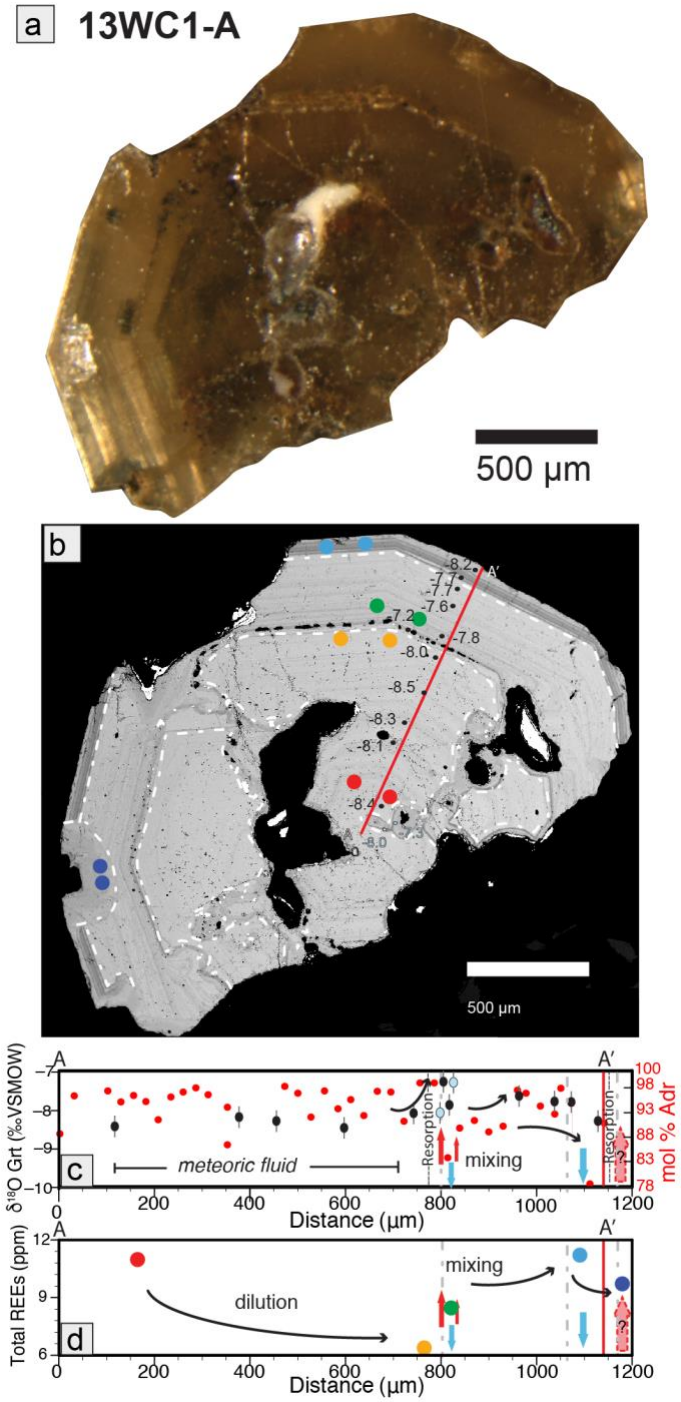

Fig. 4 Geochemistry and $\delta_{18}O$ values of garnet A from sample 13WC8; (a) Binocular, transmitted light (color) image of a polished fragment of garnet (white dotted line indicates epoxy covering the crystal), showing the zoned green andradite core, which appears yellow, with small dark magnetite inclusions aligned with growth zones, and the unzoned red-orange andradite overprint rim with scattered small (<5 µm) scheelite inclusions, not visible. (b) Backscattered electron (BSE) image of garnet zoning. Galena is a square bright mineral in the resorbed core in the backscatter image. Small (<10 µm) inclusions of magnetite and scheelite are

present, with magnetite restricted to the inner, zoned portion of the garnet (before B' along the transect) and scheelite more common in the outer overprinted area (from B to B' on the transect). White and light blue spots (to locate the blue, out of line spots along the plotted transect) with numbers represent SIMS spot locations and measured $\delta_{18}O$ values, plotted in (c). Colored spot pairs represent LA-ICPMS spot pairs along the transect, with ∑REE plotted in (d). Dash-dot white lines indicate resorption features or irregular wavy zoning visible in the backscatter image, and are copied onto transects in the following plots. (c) $\delta_{18}O$ measured by SIMS as black or light blue spots with gray error bars (barely bigger than spots) on the left axis, and corresponding mole percent andradite represented by red circles on the right axis, by distance from core to rim (in microns, μm) shows variability. Red, blue and black arrows are interpreted fluid behavior, tracking $\delta_{18}O$. (d) ∑REE concentration measured by LA-ICPMS, as a sum of REEs (La through Lu) in ppm for each analysis pair, plotted along the same transect

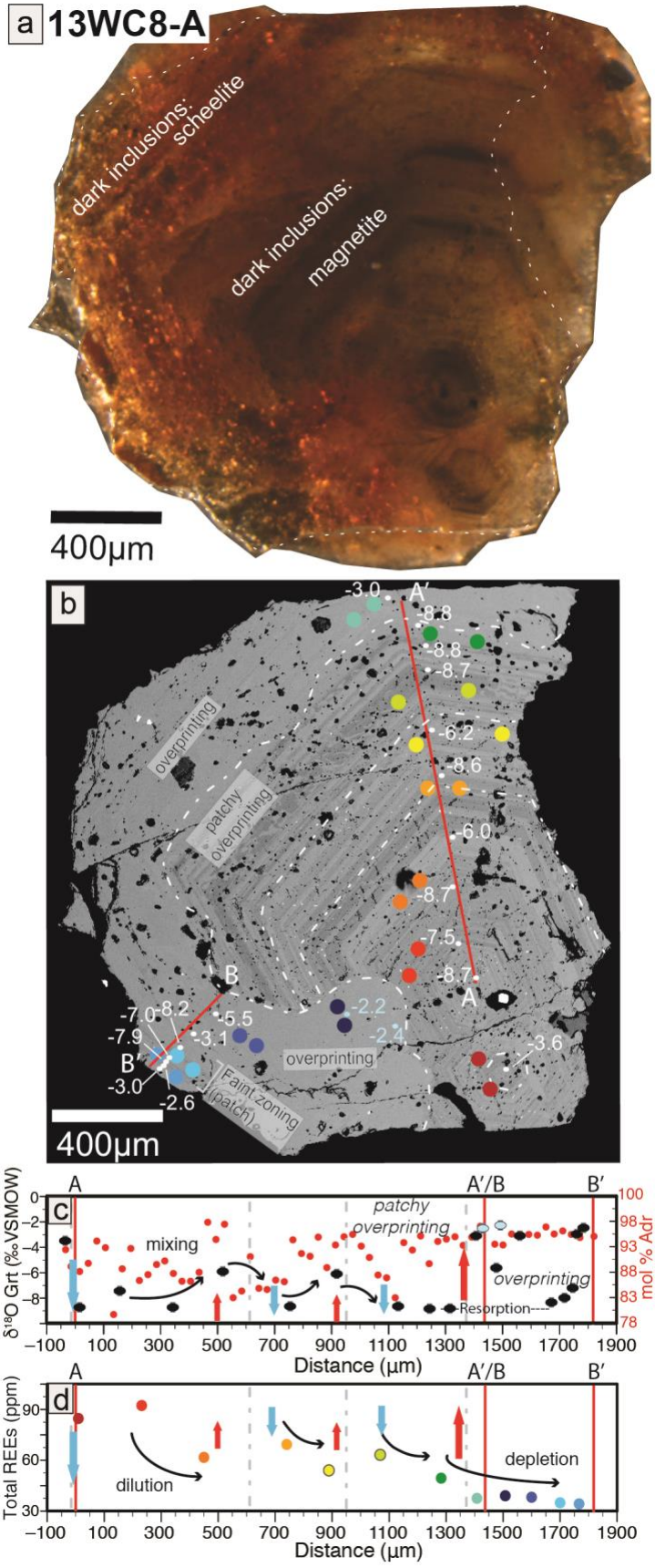
a 13WC8-A
dark inclusions: scheelite
dark inclusions: magnetite
400µm
b
A′
A
B
B′
-3.0
-8.8
-8.8
-8.7
-6.2
-8.6
-6.0
-8.7
-7.5
-8.7
-7.0
-8.2
-7.9
-3.0
-2.6
-5.5
-3.1
-2.2
-2.4
-3.6
overprinting
patchy overprinting
overprinting
Faint zoning (patch)
400µm
c
A
A′/B
B′
patchy overprinting
mixing
overprinting
Resorption
δ18O Grt (‰VSMOW)
mol % Adr
Distance (µm)
d
dilution
depletion
Total REEs (ppm)
Distance (µm)

Fig. 5 Geochemistry and $\delta_{18}O$ values of garnet A from sample 13WC1; (a) Binocular, transmitted light (color) image of garnet zoning, showing the green zoned garnet, which appears yellow, with small dark magnetite inclusions aligned with growth zones, and some white/reflective calcite, sphalerite and galena in resorbed cores. (b) Backscatter electron (BSE) image of garnet zoning, annotated with a red transect line from core to rim (A-A'). Late galena followed by sphalerite is the bright mineral at the rim and in resorbed spaces in the BSE image. Small (<10 μm) inclusions of magnetite and scheelite are sparse in the innermost section (before ~800 μm along the transect) of the garnet. Black and light blue spots (to locate the blue, out of line spots along the plotted transect) with numbers represent SIMS spot locations and measured $\delta_{18}O$ values, plotted in (c). Colored spot pairs represent LA-ICPMS spot pairs along the transect, with ∑REE plotted in (d). Dash-dot white lines indicate resorption features or irregular wavy zoning visible in the backscatter image, and are copied onto transect plots. (c) Plot of $\delta_{18}O$ measured by SIMS (black or light blue spots with gray error bars) on the left axis, and corresponding mole percent andradite (red circles) on the right axis, by distance from core to rim (in microns, μm). Red, blue and black arrows are interpreted fluid behavior, tracking $\delta_{18}O$; the red arrow with a dashed outline and question mark is an increase in magmatic fluid interpreted from ∑REE, plotted in (d), with no corresponding $\delta_{18}O$ spot. (d) ∑REE concentration in garnet measured by LA-ICPMS (La through Lu) in ppm for each analysis pair measured for a particular zone, plotted along the same transect line

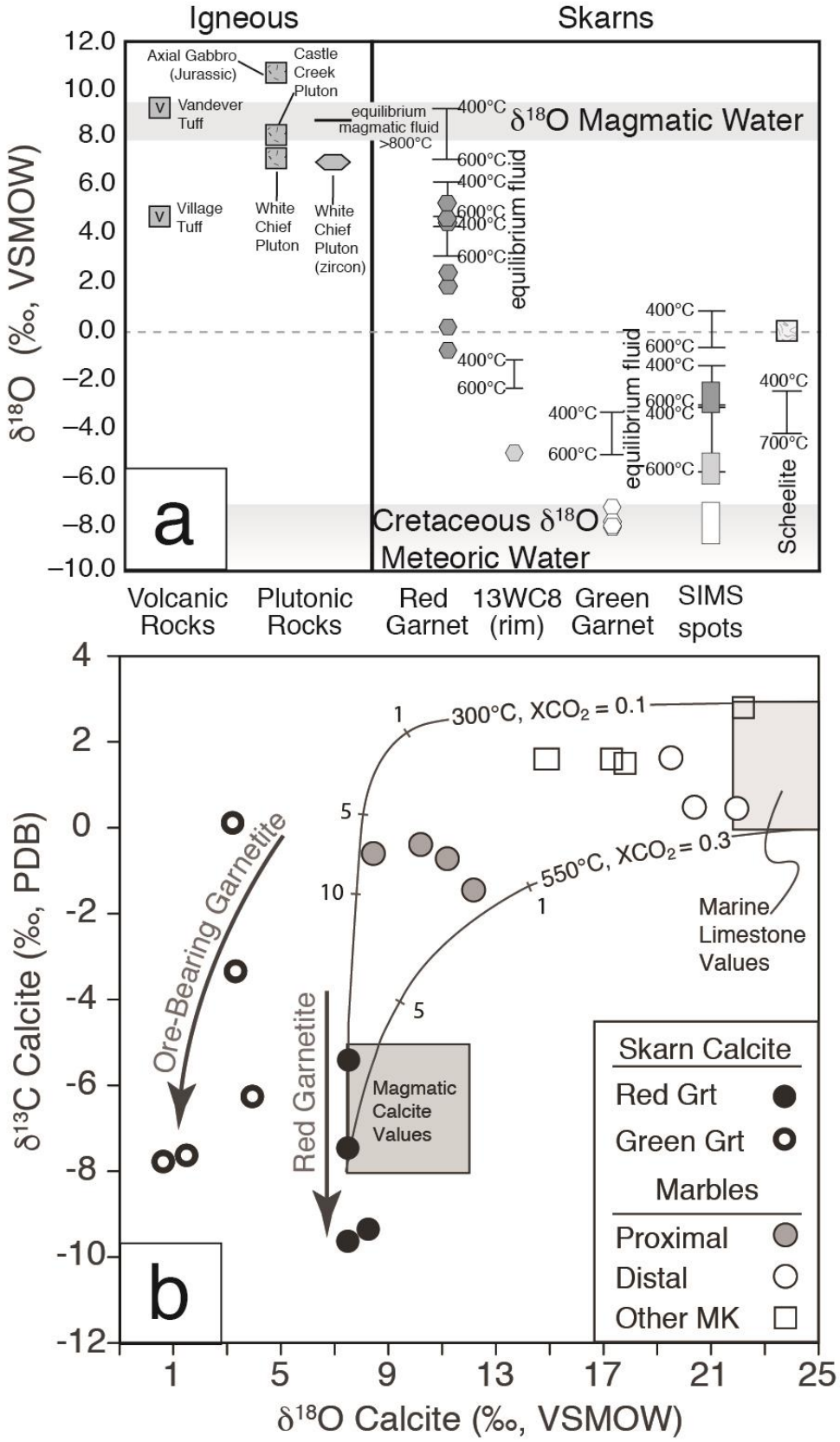
Igneous
Skarns
Axial Gabbro (Jurassic)
Castle Creek Pluton
Vandever Tuff
Village Tuff
White Chief Pluton
White Chief Pluton (zircon)
equilibrium magmatic fluid >800°C
δ18O Magmatic Water
equilibrium fluid
Cretaceous δ18O Meteoric Water
Scheelite
δ18O (‰, VSMOW)
a
Volcanic Rocks
Plutonic Rocks
Red Garnet
13WC8 (rim)
Green Garnet
SIMS spots
300°C, XCO2 = 0.1
550°C, XCO2 = 0.3
Ore-Bearing Garnetite
Red Garnetite
Magmatic Calcite Values
Marine Limestone Values
Skarn Calcite
Red Grt
Green Grt
Marbles
Proximal
Distal
Other MK
δ13C Calcite (‰, PDB)
δ18O Calcite (‰, VSMOW)
b

Fig. 6 Oxygen isotope ratios from White Chief skarn and related rocks. (a) $\delta_{18}O$ values of whole rock powders from plutonic and volcanic rocks, garnet fragments, and scheelite. Black capped lines represent calculated $\delta_{18}O$ values of equilibrium fluid over a range in temperatures from 400°C to 600°C. The $\delta_{18}O$ value of fluid is calculated to a wider range of 700 to 400°C for scheelite, as the temperature of its formation, later than garnet, is uncertain. For sample 13WC8, with the widest range in $\delta_{18}O$(Grt) measured by SIMS, the ranges of values are represented by rectangles—the white and light gray rectangles represent analyses within zoned green andradite cores, the dark gray rectangle represents analyses of the red overprint rim. (b) $\delta_{18}O$ and $\delta_{13}C$ values of calcite from marbles and skarn from the White Chief hydrothermal system. Distal marbles are massive and grey with carbonaceous matter from the White Chief area, and white squares represent samples from other areas of the pendant (Other MK). Calcite from skarn garnetite is distinguished as ore-bearing (with green garnet, thick black empty circles) and ore-absent (with red garnet, black filled circles). Reference values of marine carbonates and "magmatic calcite" calculated from equilibrium fluid fractionation are fitted with box-models for the total system assuming equilibrium carbon isotope exchange of fluid over a range of temperatures. Model curves are calculated according to Bowman (1998a, Equation 9) and assume equilibrium fractionation between calcite end-members in marine limestone ($\delta_{18}O$ = 21 to 25‰; $\delta_{13}C$ = 0 to 3‰) and water-rich fluids [X_{CO2} = 0.1 (300°C); 0.3 (550°C)] from which calcite in equilibrium with magmatic fluid ($\delta_{18}O$(Cc) = 7.5‰; $\delta_{13}C$(Cc) = –8.0) would precipitate. End-member values are from Bowman (1998a). Hash marks on model curves are fluid-rock ratios used in the models, but likely far underestimate actual fluid fluxes (Bowman 1998a; Baumgartner and Valley, 2001)

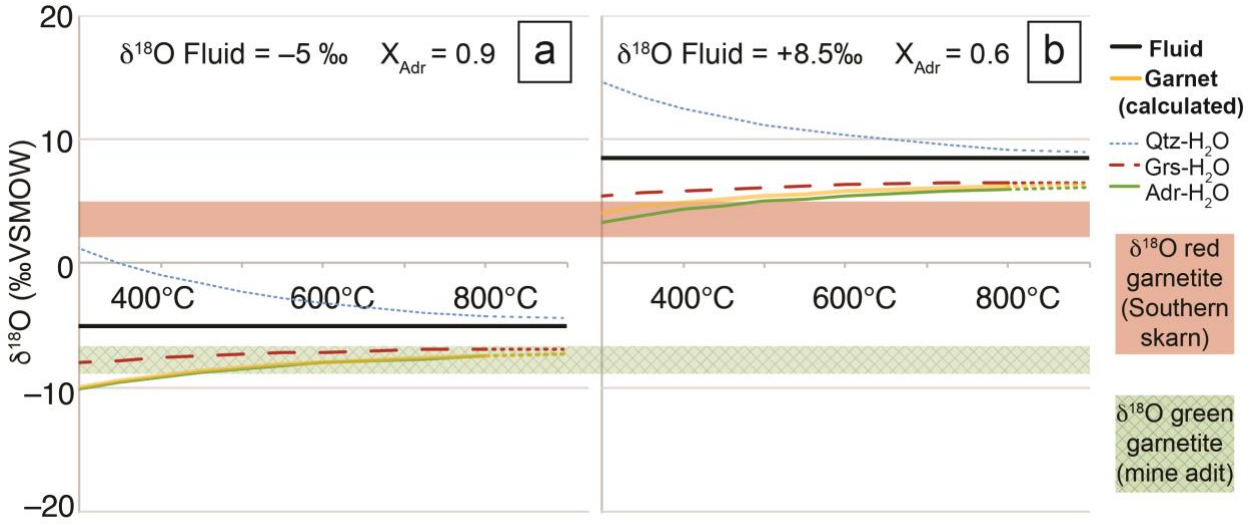

Fig. 7 Oxygen isotope fractionations and measured values for garnet relevant to the White Chief Canyon skarn system, where the thick black line represents a given water $\delta_{18}O$ value (X_{CO2} = 0), and the curves are calculated equilibrium compositions for quartz (dotted blue line), grossular garnet ($Gros_{100}$, dashed red line) and andradite (Adr_{100}, solid green line). The measured values of $\delta_{18}O$(Grt) in red and green garnets, respectively, are plotted as horizontal bars across both panels. (a) A meteoric water-rich fluid $\delta_{18}O$ of –5‰, where garnets are nearly pure andradite (yellow curve, X_{Adr} = 0.9), as seen in green ore-zone garnet. The yellow curve here nearly overlaps the equilibrium andradite curve, in green, and overlaps with measured green garnetite $\delta_{18}O$(Grt)

values to temperatures as low as ~400°C, corresponding well to the minimum temperature of 400°C from fluid inclusion assemblages in green garnetite. (b) Magmatic water ($\delta_{18}O$ = +8.5 calculated from zircon from the granodiorite of White Chief Mine) results in equilibrium $\delta_{18}O$(Grt) values that are above the highest measured values for the red garnetite. The yellow curve represents the calculated fractionation of Adr_{60} garnet in equilibrium with purely magmatic water ($\delta_{18}O$ = +8.5). The yellow curve just intersects the highest red garnetite measured values only at T < 400°C; instead of such a low T of formation of the skarn, it is likely that all garnets formed in fluids that contained some portion of meteoric water, which would lower the curves to meet the measured values at an appropriate skarn-forming temperature range (>400 °C, from fluid inclusion microthermometry)

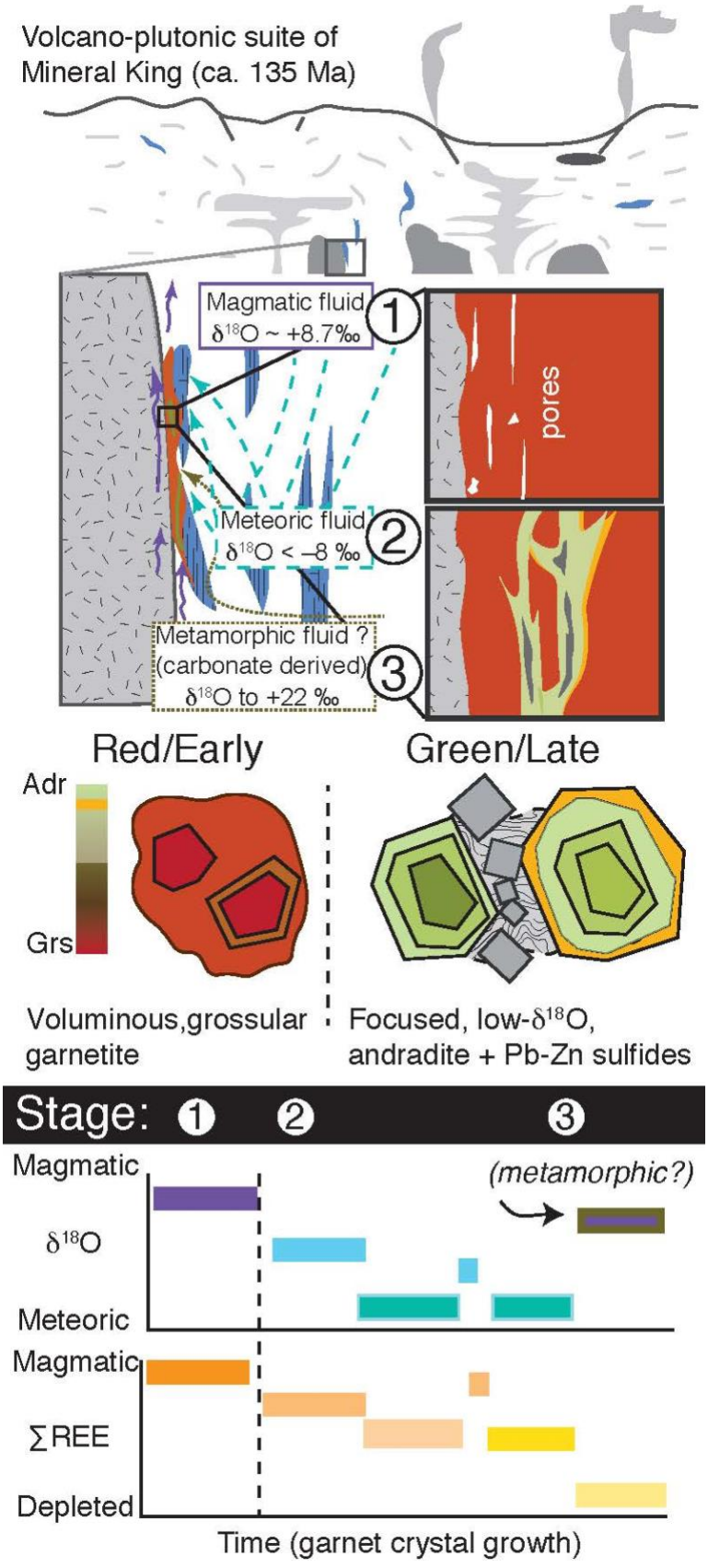
Volcano-plutonic suite of
Mineral King (ca. 135 Ma)
Magmatic fluid
δ18O ~ +8.7‰
1
pores
Meteoric fluid
δ18O < –8 ‰
2
Metamorphic fluid ?
(carbonate derived)
δ18O to +22 ‰
3
Red/Early
Green/Late
Adr
Grs
Voluminous,grossular
garnetite
Focused, low-δ18O,
andradite + Pb-Zn sulfides
Stage: 1 2 3
Magmatic
δ18O
Meteoric
(metamorphic?)
Magmatic
∑REE
Depleted
Time (garnet crystal growth)

Fig. 8 Schematic model of skarn formation at White Chief Mine. In the extensional arc setting of ca. 135 Ma, this shallow system drove convection of meteoric fluids into the skarn-forming hydrothermal system at the contact of the pluton with carbonates. Silicic magma of the granodiorite of White Chief Mine intruded carbonate, causing devolatilization of CO_2:H_2O fluid, which was first dominantly magmatic fluid (1). The opening of pore space along the contact formed a conduit for later fluids, *i.e.,* meteoric water (2), and potentially also including metamorphic fluid in equilibrium with local carbonates (3?).

Early red grossular-rich garnet crystallized in the southern present-day exposures of the skarn, with the highest $\delta^{18}O$(Grt) measured, up to > 4‰, and elevated ∑REE. Magmatic fluid ($\delta^{18}O$ of ~+8.5‰) dominated the early red garnet growth, but a significant proportion of meteoric fluid was certainly present (see Figure 7). Diminishing expulsion of magmatic water later allowed low-$\delta^{18}O$ meteoric fluid ($\delta^{18}O$ of –5‰) to flood the system, recorded by low-$\delta^{18}O$, moderate-∑REE green, oscillatory zoned garnet in the ore zone near where abandoned mine adits exist today ($\delta^{18}O$(Grt) < –8‰). Resorption and overprinting of some green zoned garnet cores resulted in red-orange andradite (Adr_{93}) overprinted rims of the garnet during the low-temperature (as low as ~400°C) skarn formation during final stages of cooling of the granodiorite of White Chief Mine, recording pulses of higher-$\delta^{18}O$, low ∑REE fluid (brown and purple bar in $\delta^{18}O$ plot, and pale yellow bar in ∑REE plot), likely a signature of "metamorphic" fluids from regional carbonate rock ($\delta^{18}O$ up to +22‰), recorded by a prominent increase in $\delta^{18}O$(Grt) (> –3‰) and extremely depleted ∑REE within the red-orange andradite garnet rims

Table 1 Oxygen and carbon isotope laser fluorination analyses (all values reported in units of permil, ‰, relative to VSMOW)

White Chief Skarn Samples					
Sample	**$\delta_{18}O$ (Grt)**	**$\delta_{18}O$ (Cc)**	**$\delta_{13}C$ (Cc)**	**Lab**	**Sample description**
13WC1	–7.6			UT	Green garnetite
13WC4	–8.4	—	—	UT	Green garnetite
13WC8-R	–4.9	1.5, 0.6	–7.6, –7.8	UT	Red-orange garnet in massive green garnetite
13WC14-G	–8.4	—	—	UT	Green-brown garnet in garnetite
13WC-22	–1.3	3.3	–3.4	UW	Green garnetite domain
14WC-9B	1.9	—	—	UW	Red garnetite
14WC-9E	—	3.2	0.1	UW	Coarse grained red garnetite; vug fill calcite
14WC-10A	2.5	7.5	–7.5	UW	Red garnet-pyroxene skarn, vug fill calcite
14WC-11A	4.5	7.5	–5.4	UW	Red garnetite, adjacent calcite marble domain
14WC-12D	4.6	8.3	–9.4	UW	Red garnetite, calcite in vugs
14WC-13 Red	0.2	3.9	–6.3	UW	Red garnetite, gradational to green, in marble
14WC-13 Olive	–8.1	—	—	UW	Red garnetite, gradational to green, in marble
14WC-14	5.1	7.5	–9.6	UT	Red garnetite; calcite in veins
White Chief Marble Samples					
Sample		**$\delta_{18}O$ (Cc)**	**$\delta_{13}C$ (Cc)**	**Lab**	**Sample description**
13WC-3	—	10.2, 8.4	–0.4, –0.6	UT	Marble, bleached white, adjacent to skarn
14WC-3	—	12.2	–1.5	UT	1 m blue-gray marble, surrounded by calc silicates
14WC-5	—	20.4	0.5	UT	Massive marble, light gray
14WC-6	—	22.0	0.4	UT	Marble, light gray
14WC-7	—	19.5	1.6	UT	Marble, bleached white
14WC-15	—	11.2	–0.7	UT	Marble, bleached white, proximal to skarn
Other samples					
Sample	**$\delta_{18}O$**	**Material**			**Sample description**
13WC12	–0.0	Scheelite	—	UT	Scheelite from green garnetite
SQMK-1	5.9	Garnet	—	UT	Sequoia Claim skarn by 98 Ma Grd of Castle Creek.
13WC-Grd	6.9, 7.0	Zircon	—	UW	Granodiorite of White Chief Mine
13WC-Grd	7.2	Whole Rock	—	UW	Granodiorite of White Chief Mine
11MK02	9.3	Whole Rock	—	UW	Vandever Mountain Tuff Collected from Vandever Mt. Area in Mineral King
11MK-03	4.6	Whole Rock	—	UW	R0 Tuff from Tar Gap Trail parking area north of road.
11MK-04	11.1	Whole Rock		UW	Gabbro Sill from Mineral King. Has pyrite and apatite, few zircons
11MK-08	8.1	Whole Rock		UW	98 Ma Granodiorite of Castle Creek